

Mice with a Disruption of the Imprinted *Grb10* Gene Exhibit Altered Body Composition, Glucose Homeostasis, and Insulin Signaling during Postnatal Life[∇]

Florentia M. Smith,^{1†} Lowenna J. Holt,^{2†} Alastair S. Garfield,¹ Marika Charalambous,^{1‡} Françoise Koumanov,¹ Mark Perry,³ Reto Bazzani,¹ Steven A. Sheardown,⁴ Bronwyn D. Hegarty,⁵ Ruth J. Lyons,² Gregory J. Cooney,⁵ Roger J. Daly,² and Andrew Ward^{1*}

University of Bath, Developmental Biology Program and Centre for Regenerative Medicine, Department of Biology and Biochemistry, Claverton Down, Bath BA2 7AY, United Kingdom¹; Cancer Research Program, Garvan Institute of Medical Research, St. Vincent's Hospital, Sydney, NSW 2010, Australia²; Departments of Anatomy and Academic Rheumatology, University of Bristol Vet School, Southwell St., Bristol BS2 8EJ, United Kingdom³; GlaxoSmithKline Pharmaceuticals, New Frontiers Science Park (North), Third Avenue, Harlow, Essex CM19 5AW, United Kingdom⁴; and Diabetes and Obesity Research Program, Garvan Institute of Medical Research, St. Vincent's Hospital, Sydney, NSW 2010, Australia⁵

Received 8 November 2006/Returned for modification 14 December 2006/Accepted 22 May 2007

The Grb10 adapter protein is capable of interacting with a variety of receptor tyrosine kinases, including, notably, the insulin receptor. Biochemical and cell culture experiments have indicated that Grb10 might act as an inhibitor of insulin signaling. We have used mice with a disruption of the *Grb10* gene (*Grb10*Δ2-4 mice) to assess whether Grb10 might influence insulin signaling and glucose homeostasis in vivo. Adult *Grb10*Δ2-4 mice were found to have improved whole-body glucose tolerance and insulin sensitivity, as well as increased muscle mass and reduced adiposity. Tissue-specific changes in insulin receptor tyrosine phosphorylation were consistent with a model in which Grb10, like the closely related Grb14 adapter protein, prevents specific protein tyrosine phosphatases from accessing phosphorylated tyrosines within the kinase activation loop. Furthermore, insulin-induced IRS-1 tyrosine phosphorylation was enhanced in *Grb10*Δ2-4 mutant animals, supporting a role for Grb10 in attenuation of signal transmission from the insulin receptor to IRS-1. We have previously shown that Grb10 strongly influences growth of the fetus and placenta. Thus, Grb10 forms a link between fetal growth and glucose-regulated metabolism in postnatal life and is a candidate for involvement in the process of fetal programming of adult metabolic health.

Insulin controls glucose homeostasis by regulating protein, lipid, and carbohydrate metabolism. Cellular responses to insulin in target tissues, such as skeletal muscle, adipose tissue, and liver, are mediated via the insulin receptor (Insr) (reviewed in reference 51). Activation of the Insr results in tyrosine phosphorylation of intracellular docking proteins such as Shc and IRS-1 through IRS-4, which then bind specific Src homology 2 (SH2) domain-containing enzymes and adaptors, leading to the activation of downstream signaling cascades. A critical event mediating insulin regulation of metabolic endpoints is the activation of phosphatidylinositol 3-kinase (PI3K). This stimulates the synthesis of phosphatidylinositol 3,4,5-triphosphate, which induces plasma membrane recruitment and subsequent phosphorylation of protein kinase B (also known as Akt), a key player in the regulation of glucose uptake

and glycogen synthesis. Activation of the Insr and downstream signaling results in increased glucose uptake, utilization, and storage in adipose tissue and skeletal muscle, while decreased gluconeogenesis and glycogenolysis and increased glycogen synthesis occur in the liver (reviewed in reference 51). Resistance to these effects of insulin is a defining feature of type 2 diabetes, a polygenic disease afflicting over 110 million people worldwide. Impaired insulin action is also a feature of obesity and predisposes people to arteriosclerosis and cardiovascular diseases, facts which highlight its importance in human health. The fundamental role of the Insr in insulin action was demonstrated following targeted disruption of the receptor (1, 29). To dissect the contribution of individual tissues to glucose homeostasis, and to overcome the lethal phenotype of *Insr* knockout (KO), tissue-specific *Insr* KO mutants have been generated. These experiments have uncovered novel functions of the Insr in tissues such as brain and pancreatic β cells (reviewed in reference 31).

Grb10 belongs to a family of related signaling adaptor proteins that also includes Grb7 and Grb14 (24, 27). These Grb7 family proteins each have an N-terminal region harboring a conserved proline-rich motif, a central region containing a pleckstrin homology (PH) domain and a C-terminal SH2 domain. A novel domain has also been identified in these proteins, termed the BPS (between PH and SH2) domain, which

* Corresponding author. Mailing address: University of Bath, Developmental Biology Program and Centre for Regenerative Medicine, Department of Biology and Biochemistry, Claverton Down, Bath BA2 7AY, United Kingdom. Phone: 00(44)1225 386914. Fax: 00(44)1225 386779. E-mail: bssaw@bath.ac.uk.

† These authors have contributed equally to this work.

‡ Present address: Department of Physiology, Development and Neuroscience, University of Cambridge, Anatomy Building, Downing Street, Cambridge CB2 3BY, United Kingdom.

[∇] Published ahead of print on 11 June 2007.

can contribute to receptor interactions (17, 25, 30). Originally identified through its ability to bind to the epidermal growth factor receptor, Grb10 has been shown to bind both the Insr and the related type 1 insulin-like growth factor receptor (IGF1R), as well as a number of other receptor tyrosine kinases (27). The functional role of Grb10 in insulin signaling is controversial, with some studies demonstrating stimulatory effects on biological endpoints while the majority indicate an inhibitory role. Grb10 exhibited ligand-inducible association with the activated Insr in vitro, by virtue of its BPS and SH2 domains (25, 57). Furthermore, overexpression of Grb10 in CHO cells overexpressing the human INSR inhibited insulin-induced tyrosine phosphorylation of downstream signal transducing proteins such as IRS-1, leading to inhibition of subsequent association with PI3K (38). Recent studies have suggested a Grb10-mediated inhibition of insulin signaling resulting from a physical disruption of IRS association with phosphorylated residues of the Insr (63). In addition, GRB10 overexpression in rat hepatocytes resulted in inhibition of insulin-stimulated glycogen synthase via a proposed novel pathway (44). While some experiments have shown Grb10 to be a positive regulator of both insulin and IGF1 action (16, 60), the consensus view is that Grb10 may function to inhibit insulin signaling or to redirect the Insr signaling pathway (reviewed in reference 27).

While the role of Grb7 in insulin signaling is largely unexplored, Grb14 has also been strongly implicated in insulin signaling in a number of studies (reviewed in reference 27). For example, overexpression of Grb14 in CHO-IR cells was shown to inhibit insulin-induced tyrosine phosphorylation of IRS-1 while repressing insulin-stimulated mitogenesis and glycogen synthesis (30). Consistent with a role for Grb14 as an inhibitor of insulin signaling, microinjection of Grb14 resulted in inhibition of insulin-induced *Xenopus* oocyte maturation (10). The most compelling evidence for the physiological role of Grb14 has come from gene KO studies of mice. Disruption of *Grb14* in mice resulted in hypoinsulinemia and improved glucose tolerance indicative of enhanced insulin sensitivity (15). Following in vivo insulin stimulation, livers and muscles of *Grb14* KO mice exhibited enhanced insulin signaling via IRS-1 and Akt and increased incorporation of glucose into glycogen, while effects on insulin action were not detected in adipose tissue of the same mice. These observations establish Grb14 as a tissue-specific inhibitor of insulin signaling. A recent structural study provides a mechanistic explanation for these observations, revealing that the Grb14 BPS domain functions as a pseudosubstrate inhibitor of the Insr kinase (17). Interestingly, an additional role for Grb14 is to protect the Insr activation loop from dephosphorylation by specific protein tyrosine phosphatases (PTPs), while indirectly promoting dephosphorylation of Y972 and thereby reducing recruitment of IRS-1 (15, 46).

Grb10 is an imprinted gene, setting it apart from the other *Grb7* family members (43). Expression of *Grb10* occurs predominantly, though not exclusively, from the maternal allele, and we have shown previously that disruption of the maternal *Grb10* allele in mice results in significant embryonic and placental overgrowth (12). Several imprinted genes are known to influence fetal and postnatal growth and collectively form a significant proportion of those genes currently identified as

exerting major effects on whole-body size and proportions. A number of imprinted genes have also been shown to have roles in the regulation of glucose-regulated metabolism (reviewed in reference 55).

To elucidate the role of *Grb10* in adult life and dissect the signaling pathways it regulates in a physiological setting, we used mice with a disruption in the *Grb10* genomic locus, termed *Grb10 Δ 2-4* (12). As Grb10 has been strongly implicated in insulin signaling, experiments were aimed at addressing the potential role of this adapter protein in Insr signaling and glucose homeostasis in vivo. Adult *Grb10 Δ 2-4* mice were found to have an increased muscle mass and reduced adiposity, together with improved glucose clearance and tissue-specific changes in insulin-induced Insr and IRS-1 tyrosine phosphorylation. Similar changes were observed at the IGF1R, and at the level of IRS-1 tyrosine phosphorylation, in response to IGF1. These findings indicate that Grb10 modulates Insr/IRS-1 signaling in a manner similar to that of Grb14 but with a different tissue specificity. However, unlike Grb14, Grb10 exerts an additional control over body composition that may contribute significantly to the metabolic phenotype.

MATERIALS AND METHODS

Mice. All mice were housed under standard conditions as described previously (5). *Grb10 Δ 2-4* mice were maintained for several generations on a mixed C57BL/6 \times CBA genetic background and were genotyped using PCR assays (see reference 12). Experiments were carried out with the approval of the Garvan Institute/St. Vincent's Hospital Animal Ethics Committee, following guidelines issued by the National Health and Medical Research Council of Australia, or were approved by the University of Bath ethical committee and carried out under license from the United Kingdom Home Office.

Analysis of tissue weights, gene expression, and histology. Mice were killed by cervical dislocation, tissues were dissected free and dabbed briefly on paper towels to remove excess fluid, and wet weights were recorded immediately. Tissues were analyzed for β -galactosidase gene expression as previously described (5). Histological sections were cut from tissues embedded in paraffin wax and subsequently stained with hematoxylin and eosin according to standard procedures. Sections were viewed under a DMRB compound microscope (Leica Microsystems, Bensheim, Germany) and images captured using a SPOT RT camera and Advanced Spot RT 3.0 (Diagnostic Instruments, MI) software.

DXA analysis. Adult mice killed by cervical dislocation were analyzed by dual-energy-X-ray absorptiometry (DXA) using a PIXImis scanner (Lunar, Madison, WI) with small-animal software, as previously described (40). The parameters that were evaluated included total area, lean tissue weight, and fat tissue weight. Lean and fat tissue weights were then expressed as percentages of total body weight prior to statistical analysis.

Leptin measurements. Serum leptin concentrations were determined using a mouse leptin enzyme-linked immunosorbent assay kit (Crystal Chem Inc., IL), as per the manufacturer's instructions, with absorbance measured with a TECAN Spectra plate reader.

Monitoring of food consumption. Prior to the onset of food consumption measurements, mice were caged individually and allowed 1 week to adjust to recaging. At day 1 of the study, animals and their food were weighed. Over a period of 3 to 4 weeks, food consumption was assessed by weighing the food and the mice at five time points at the same time of day to calculate the amount of food consumed per gram of body weight per day.

GTT and ITT. Glucose tolerance tests (GTT) and insulin tolerance tests (ITT) were performed to assess whole-body glucose metabolism. The GTT (2 g glucose given intraperitoneally [i.p.]/kg of body weight) and ITT (0.75 U insulin given i.p./kg) were performed on mice fasted overnight (approximately 16 h) that were matched for age and sex. Blood samples were obtained from the tail tip at the times indicated. Glucose concentrations were determined using either One-Touch ULTRA (Lifescan, CA) or Accu-CHEK II (Roche Diagnostics Corporation, Basel, Switzerland) glucometers. For plasma measurements, blood was collected into tubes and centrifuged at 13,000 rpm for 10 min, with plasma transferred to a fresh tube prior to analysis. Plasma insulin concentrations were assayed using an ultrasensitive enzyme-linked immunosorbent assay kit (Merco-

dia AB, Uppsala, Sweden). The IGF1 concentration in plasma was determined by immunoenzymic assay (IDS).

Assessment of glucose dispersal to tissues. GTT were performed with trace amounts of 2-[³H]DOG (deoxyglucose) and [U-¹⁴C]glucose to determine the clearance of 2-[³H]DOG into various tissues as indicated or the clearance of [U-¹⁴C]glucose into glycogen or lipid, respectively. Trace amounts of 2-[³H]DOG and [U-¹⁴C]glucose were mixed with 50% glucose in normal saline and injected into mice who fasted overnight (2 g glucose i.p./kg, 10 μ Ci/animal). During this radiolabeled GTT, blood was collected from the tail tip at various time points. Blood glucose and blood radioactivity were determined at each time point, and the area under the curve was calculated in both cases. At the end of the time course (90 min), the animals were sacrificed by cervical dislocation and tissues (liver, quadriceps muscle, tibialis muscle, white adipose tissue [WAT], and brown adipose tissue) collected and frozen in liquid nitrogen.

To analyze the clearance of 2-[³H]DOG into muscle and fat, tissue (30 to 50 mg) was homogenized in 1.5 ml of water with a Polytron homogenizer. The homogenate was centrifuged at 13,000 rpm for 10 min, and supernatant was collected. To determine the total counts, 200 μ l of supernatant was analyzed by liquid scintillation counting. A 400- μ l sample of the supernatant was passed through an anion exchange column (AS 1-X8 resin; Bio-Rad, CA) for determination of the free counts. Of the 6 ml of water used to wash the column, 1 ml of this was taken for analysis by liquid scintillation counting. The clearance of 2-[³H]DOG was calculated by correction for area under the curve for radioactive glucose during the GTT and for the weight of the tissue sample used.

For the determination of incorporation of radiolabeled glucose into glycogen, tissue samples of the liver and muscle (~50 mg) were digested in 200 μ l of 1 M KOH at 70°C for 20 min. After the addition of 75 μ l of saturated NaSO₄, glycogen was precipitated by the addition of 1.7 ml of 95% ethanol. The pellets were washed with 95% ethanol and redissolved in 1 ml of aminoglycosidase buffer. The clearance of radioactive glucose into glycogen was assessed by liquid scintillation counting of a sample of the glycogen solution and correction for the area under the curve for radioactive glucose during the GTT as well as for the weight of the tissue sample used.

To assess the incorporation of [U-¹⁴C]glucose into lipid, WAT was homogenized overnight in chloroform-methanol (2:1). Subsequently, 0.6% NaCl was added to facilitate separation of the organic and aqueous phases. The lower organic phase (containing extractable, neutral lipids) was collected and evaporated to dryness under nitrogen gas. After the extract was redissolved in ethanol, the sample was subjected to liquid scintillation counting. The clearance of radioactive glucose into lipid was calculated, taking into account the area under the curve for radioactive glucose during the GTT, and the weights of the tissue samples were analyzed.

Analysis of Insr and IGF1R signaling. Mice (two to four per genotype) were fasted overnight and were anesthetized by injection of 30 mg pentobarbitone/kg. The peritoneal cavity was opened and recombinant human insulin (1 unit/kg) or IGF1 (0.25 mg/kg; GroPep, Adelaide, Australia) was injected into the inferior vena cava, following previously established protocols (the insulin protocol is described in reference 15 and the IGF1 protocol is described in reference 35). After 2 min (by the insulin protocol) or 5 min (by the IGF1 protocol), WAT, quadriceps muscles, and tibialis muscles were collected and immediately frozen in liquid nitrogen. The tissues were solubilized (after powdering, in the procedure for muscles) for 2 h at 4°C in modified radioimmunoprecipitation assay buffer (65 mM Tris, 150 mM NaCl, 5 mM EDTA, 0.1% Nonidet P-40, 0.5% sodium deoxycholate, 0.1% sodium dodecyl sulfate, 10% glycerol, pH 8.0) supplemented with protease and phosphatase inhibitors (10 μ g/ml aprotinin, 10 μ g/ml leupeptin, 20 mM NaF, 1 mM Na orthovanadate, 1 mM phenylmethylsulfonyl fluoride). Cleared tissue lysates were resolved by sodium dodecyl sulfate-polyacrylamide gel electrophoresis and immunoblotted with antibodies against the Insr β subunit (BD Transduction Laboratories, CA), IGF1R β subunit (Santa Cruz Biotechnology Inc.), phosphorylated Insr/IGF1R (pY1162/3 and pY972; Biosource, CA), phosphotyrosine (clone 4G10; Upstate, Charlottesville, VA), IRS-1 (Upstate), phospho-IRS-1/2 (pY612, Biosource), and Akt or phospho-Akt (pS473 or pT308) (Cell Signaling Technology, Danvers, MA). Note that the pY1162/3 antibody detects both phosphorylated Insr and IGF1R β subunits, and the two receptors can be separated on polyacrylamide gels, with IGF1R migrating more slowly than Insr (see reference 34). In most immunoprecipitation experiments, the Insr was first immunoprecipitated from lysates by using a monoclonal antibody (Ab3; Oncogene Research Products, Darmstadt, Germany). In the case of coimmunoprecipitation of Insr and Grb10, the Insr was immunoprecipitated using a different monoclonal antibody (L55B10; Cell Signaling, CA) and Grb10 was detected using a rabbit polyclonal antibody (K20; Santa Cruz, CA). Note that in these experiments, tissue samples were collected from free-fed animals that had not been stimulated with insulin. Quantitation of

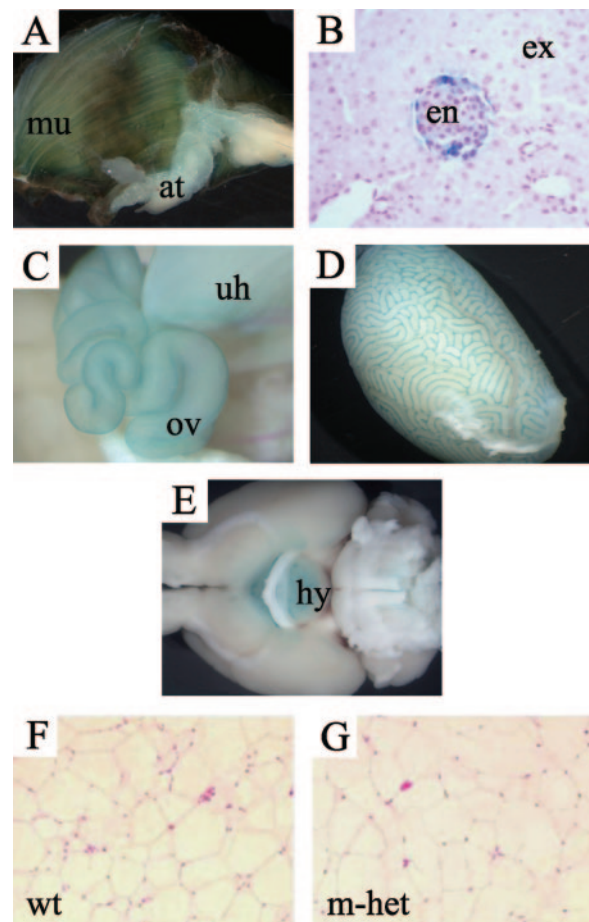


FIG. 1. Expression of *Grb10* in adults is imprinted and restricted to a limited set of tissues. Adult organs were collected following maternal (*Grb10* Δ 2-4^{mv/+}) or paternal (*Grb10* Δ 2-4^{+/p}) transmission of the *Grb10* Δ 2-4 allele and stained for β -galactosidase activity (blue staining). β -Galactosidase was expressed exclusively from the maternal allele in the skeletal muscle (mu) and adipose tissue (at) (A), endocrine pancreas (en) (B), oviduct (ov) and uterine horns (uh) (C), and Leydig cells of the testes (D). The exocrine pancreas is also shown. No expression was detected from the paternal allele in these tissues. (E) *Grb10* was expressed from the paternal allele in the hypothalamus (hy), while no expression was detected from the maternal allele at this site. (F and G) WAT histology showing no major differences between wild type (wt) and *Grb10* Δ 2-4^{mv/+} (m-het) mouse samples.

immunolabeled bands was performed using immunoprecipitation lab gel H (BD Biosciences, CA) or L55B10 (Cell Signaling, CA).

Statistical analysis. Results are presented as means \pm standard errors of the means (SEM). Statistical analysis was performed using either unpaired Student's *t* test or analysis of variance (ANOVA) with appropriate post hoc tests with PRISM 4.0 software (GraphPad, San Diego, CA). Differences with *P* values of <0.05 were considered to be statistically significant.

RESULTS

Imprinted and restricted expression of *Grb10* in the adult.

In our initial report on the phenotype of *Grb10* Δ 2-4 mutant mice, we focused on the fetal overgrowth leading to the birth of pups that are around 30% heavier than their wild-type littermates (12). Only mice inheriting the maternal *Grb10* Δ 2-4 mutant allele (maternal [*Grb10* Δ 2-4^{mv/+}] heterozygotes and

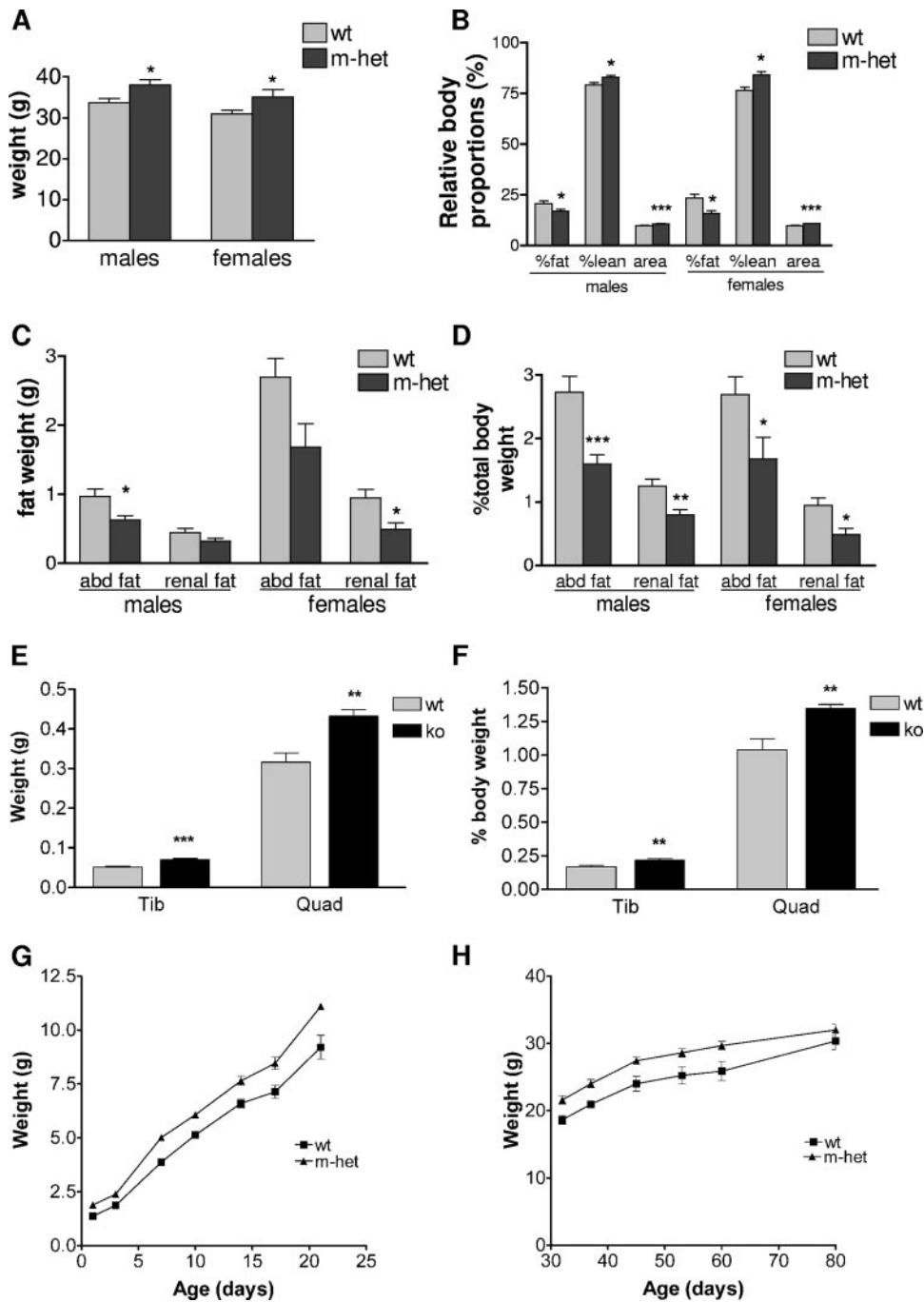


FIG. 2. Increased body weight and reduced adiposity in adult *Grb10Δ2-4^{m/+}* (m-het) mice compared to those of the wild types (wt). (A) Total body weights of male and female mice 6 months of ages. (B) DXA analysis of total body area, percent fat tissue, and percent lean tissue. (C) Absolute weights of dissected abdominal (abd) and renal fat depots. (D) Weights of dissected abdominal (abd) and renal fat pads expressed as percentages of total body weight. (E) Absolute weights of dissected tibialis (Tib) and quadriceps (Quad) muscles. (F) Weights of dissected tibialis (Tib) and quadriceps (Quad) muscles expressed as percentages of body weight. (G and H) Mean body weights of *Grb10Δ2-4^{m/+}* and wild-type animals recorded from birth to 80 days of age. Data from the same animals has been divided into preweaning (G) and postweaning (H) data, representing the rapid-growth and slow-growth periods, respectively. All results are expressed as means \pm SEM (*, $P < 0.05$; **, $P < 0.01$; ***, $P < 0.001$).

Grb10Δ2-4^{m/p} homozygotes) were affected, and the overgrowth included disproportion at the level of tissues and organs that was correlated with *Grb10* expression levels in developing tissues. The presence of the β -galactosidase-neomycin resis-

tance fusion gene cassette in the *Grb10Δ2-4* allele provides a convenient method to follow expression from the *Grb10* locus by assaying for β -galactosidase activity in situ. We previously found that reporter gene expression was widespread in the

embryo and closely followed the pattern of expression from the endogenous *Grb10* allele, as determined by mRNA in situ hybridization (12). Furthermore, expression of β -galactosidase from the *Grb10 Δ 2-4* allele was used to confirm the imprinted nature of the *Grb10* locus. Following transmission of the *Grb10 Δ 2-4* allele from either males or females, expression in the fetus was predominantly from the maternal allele.

In the present study, we have extended our expression analysis to adult stages by comparing tissues that were dissected from wild-type mice, as well as from both maternal (*Grb10 Δ 2-4^{m/+}*) heterozygotes and paternal (*Grb10 Δ 2-4^{+/p}*) heterozygotes, and stained for β -galactosidase activity (Fig. 1A to E). Following maternal transmission of the *Grb10 Δ 2-4* allele, staining was readily detectable in skeletal muscle, WAT, the intrinsic muscle of the tongue, and cells of pancreatic islets. Staining occurred throughout pancreatic islets, suggesting expression from both major endocrine cell types (α and β cells). Additionally, in females, there was distinct staining of the uterine horns and oviducts, while in male mice, β -galactosidase activity was present in the testes. When the testes were histologically examined, it appeared that the expression was restricted to the Leydig cells (not shown). We note that LacZ expression was not detected in adult liver. The only site of expression identified by β -galactosidase staining following paternal transmission of *Grb10 Δ 2-4* was the hypothalamus, the organ in which expression in maternal heterozygotes was notably absent (Fig. 1E).

Reduced adiposity following *Grb10* disruption. The mean weights of *Grb10 Δ 2-4^{m/+}* males (38.11 ± 1.226 g) and females (35.08 ± 1.84 g) at 6 months of age were around 13% greater than those of wild-type male (33.73 ± 1.067 g) and female (30.97 ± 0.8418 g) littermates (Fig. 2A). The weight differential was, for both sexes, less than the 36% increase observed on the day of birth (see reference 13) but remained statistically significant (for males, a *P* value of 0.01; for females, a *P* value of 0.035). We focused mainly on a comparison of *Grb10 Δ 2-4^{m/+}* heterozygotes and wild-type littermate controls, since disruption of the maternal allele will ablate the majority of *Grb10* expression in both the fetus and the adult. Consistent with this, we note that the analysis of *Grb10 Δ 2-4^{+/p}* and *Grb10 Δ 2-4^{m/p}* animals showed that they closely resembled wild-type and *Grb10 Δ 2-4^{m/+}* animals, respectively (including measures of body weight, proportions, and whole-body glucose metabolism; data not shown). Animals at 6 months of age were subjected to DXA to assess total body area, together with lean and fat tissue contents (Fig. 2B). The total body areas of *Grb10 Δ 2-4^{m/+}* mice were significantly increased (for males, a *P* value of 0.001; for females, a *P* value of 0.0003), indicating that these animals remain larger than their wild-type littermates as adults. However, DXA analysis also revealed a significant difference in body fat content, expressed as percent total body weight, with *Grb10 Δ 2-4^{m/+}* mice exhibiting a reduction compared to wild types (for males, a *P* value of 0.034; for females, a *P* value of 0.018). Conversely, *Grb10 Δ 2-4^{m/+}* mice had significantly greater lean tissue contents (for males, a *P* value of 0.033; for females, a *P* value of 0.021). To further investigate the lean phenotype at the tissue level, renal and abdominal WAT depots were dissected free and weights were recorded (Fig. 2C). The adipose depots of 6-month-old *Grb10 Δ 2-4^{m/+}* mice consistently weighed less than those of wild-type littermates, with significant differences seen for male abdominal (*P* = 0.045) and female renal

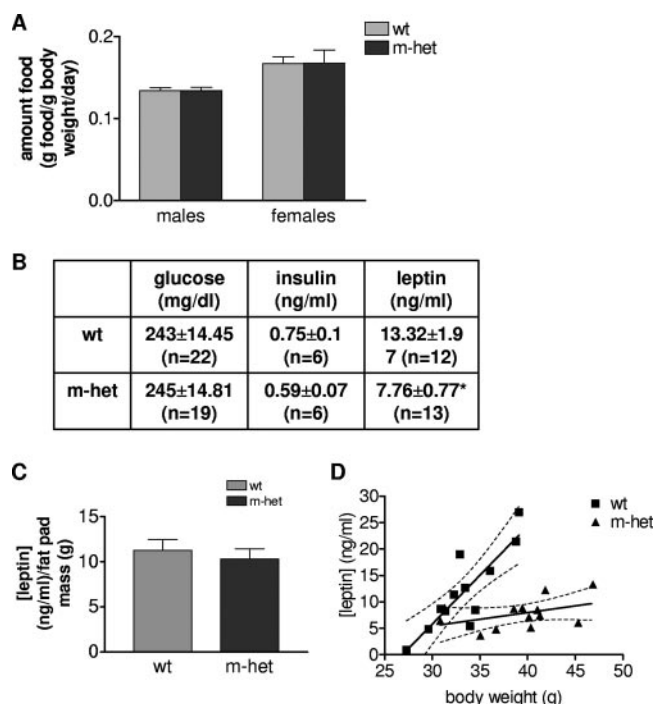


FIG. 3. Food intake and serum glucose, insulin, and leptin levels in adult *Grb10 Δ 2-4^{m/+}* (m-het) and wild-type (wt) animals. (A) Food consumption (grams food per gram of body weight per day) of 6-month-old male and female mice. (B) Serum glucose, insulin, and leptin concentrations in free-fed 6-month-old males. (C) Serum leptin concentration normalized for WAT mass. (D) Correlation between serum leptin levels and total body weight for wild-type (wt; *P* = 0.0005) and *Grb10 Δ 2-4^{m/+}* (m-het; *P* = 0.1416 [nonsignificant]) assessed using a two-tailed Spearman's rank correlation test. All results are expressed as means \pm SEM and were compared using ANOVA, except as stated for panel D (*, *P* < 0.05).

(*P* = 0.035) depots. When these weight values were expressed as percentages of total body weight (Fig. 2D), abdominal and renal fat values were in all cases significantly reduced compared to those of wild-type littermates (for males, *P* values of 0.0005 and 0.003, respectively; for females, *P* values of 0.03 and 0.035, respectively), corroborating the data obtained from DXA analysis. Similarly, tibialis and quadriceps muscles were dissected from male mice at 17 to 18 weeks of age, and those from *Grb10 Δ 2-4^{m/p}* mice were found to be significantly heavier than those from wild-type littermates (for tibialis muscles, a *P* value of 0.0006; for quadriceps muscles, a *P* value of 0.0011) (Fig. 2E); this difference was preserved when the same weight values were expressed as percentages of total body weight (for tibialis muscles, a *P* value of 0.0032; for quadriceps muscles, a *P* value of 0.0035) (Fig. 2F). To test the idea that the percent weight difference observed between wild-type and *Grb10 Δ 2-4^{m/+}* mice diminished over time and was not an artifact of studying separate cohorts of neonatal and adult mice, the postnatal weights of some animals were monitored from birth to 80 days of age (Fig. 2G and H). The results showed that the weight difference diminished mainly during the postweaning period. Histological analyses have established no obvious differences in the appearance of WAT between wild-type (Fig. 1F) and *Grb10 Δ 2-4^{m/+}* (Fig. 1G) mice at this age, and there were no significant differences in either the mean sizes of adipocytes or the

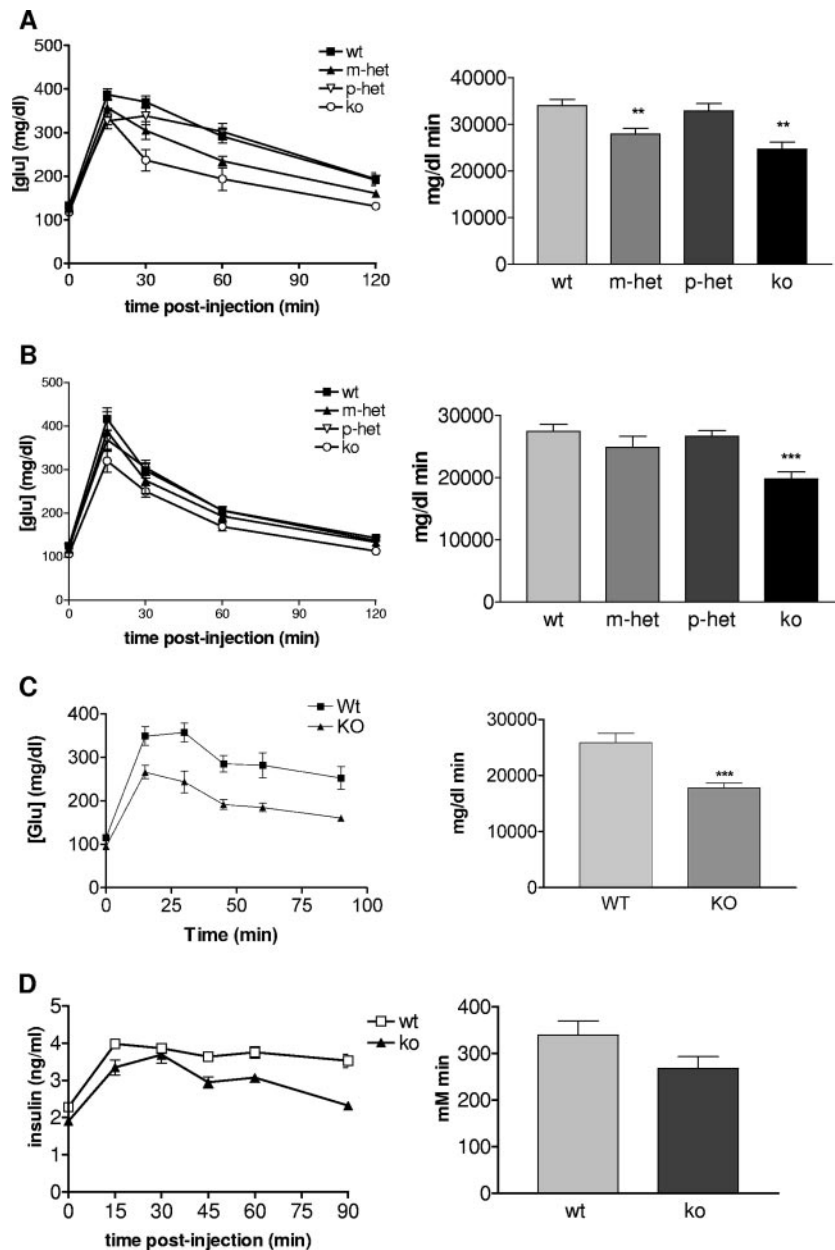


FIG. 4. Improved glucose clearance in *Grb10Δ2-4* mutant mice. Results of i.p. GTT for male (A) and female (B) mice at 10 months of age who fasted overnight are shown (left panels). *Grb10Δ2-4^{m/+}* (m-het), *Grb10Δ2-4^{p/p}* (p-het) and *Grb10Δ2-4^{m/p}* (ko) animals are compared with wild-type (wt) littermate controls. The incremental areas under the glucose curves are shown (right panels). (C) GTT for males 18 to 22 weeks of age. (D) Serum insulin concentration during a GTT. All results are expressed as means \pm SEM (*, $P < 0.05$; **, $P < 0.01$; ***, $P < 0.001$ [ANOVA]).

numbers of cells per μm^2 (data not shown). Similarly, there were no obvious differences in muscle histology (data not shown).

Food intake and glucose metabolism in *Grb10Δ2-4^{m/+}* mice.

Due to the significant decrease in adipose tissue mass observed for adult *Grb10Δ2-4^{m/+}* mice, one obvious question to ask was whether these mice demonstrated hypophagia (reduced food consumption) compared to wild-type littermates. Feeding studies were performed on cohorts of both male and female mice at 6 months of age. The results, expressed as amounts of food in grams per gram of body weight per day, indicate that the food intake of *Grb10Δ2-4^{m/+}* mice was not altered, with

amounts of daily food intake being comparable to those of wild-type animals (for males, a P value of 0.94; for females, a P value of 0.86) (Fig. 3A). At the same time, levels of serum glucose, insulin, and leptin in animals fed ad libitum were measured (Fig. 3B). There was no significant difference between the levels of glucose or insulin; however, the mean serum leptin concentration in *Grb10Δ2-4^{m/+}* mice (7.759 ± 0.7703 ng/ml; $n = 13$) was lower than that in wild-type animals (13.32 ± 1.971 ng/ml; $n = 12$), and this difference was statistically significant ($P = 0.0126$). Measurements of serum IGF1 levels in *Grb10Δ2-4^{m/p}* mice at 17 to 18 weeks and also 18 months

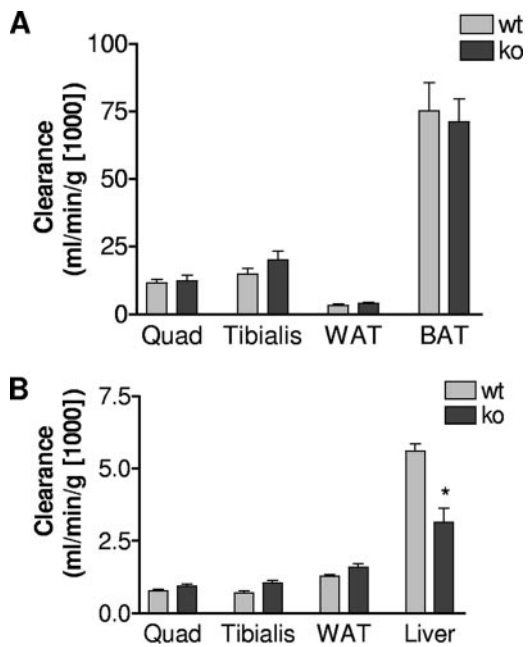


FIG. 5. Comparison of wild-type (wt) and *Grb10Δ2-4^{m/p}* (ko) male mice 18 to 22 weeks of age for clearance of 2-[³H]DOG (A) and [U-¹⁴C]glucose (B) into insulin-responsive tissues. The tissues used were quadriceps (Quad) and tibialis muscles, WAT, brown adipose tissue (BAT), and liver. All results are expressed as means ± SEM (*, *P* < 0.05 [ANOVA]).

of age were analyzed, and in both cases, these mice showed no significant difference in comparison to wild-type littermates (data not shown). The reduced serum leptin concentration could be correlated with reduced adiposity in the mutant animals, since there was no significant difference when the data were expressed

per gram of body fat for *Grb10Δ2-4^{m/+}* (12.41 ± 2.355 ng/ml/g fat) and wild-type (11.23 ± 1.236 ng/ml/g fat) mice (Fig. 3C). Furthermore, serum leptin levels were strongly correlated with body mass in wild-type animals (*P* = 0.0005), but there was no significant correlation in *Grb10Δ2-4^{m/+}* mice (*P* = 0.1416) (Fig. 3D).

Glucose tolerance in male and female mice 6 to 10 months of age, with *Grb10Δ2-4^{m/+}*, *Grb10Δ2-4^{+/p}*, and *Grb10Δ2-4^{m/p}* animals was assessed and compared with that of wild-type littermate controls (Fig. 4A and B). There were significantly improved abilities of both male and female *Grb10Δ2-4^{m/p}* mice to clear a glucose load (as judged by a reduction in the incremental area under the curve). Male and female *Grb10Δ2-4^{m/+}* animals followed the same trend, though only males were significantly different from wild-type animals, while *Grb10Δ2-4^{+/p}* animals had a glucose clearance profile that was essentially the same as that of the wild type. Most of our subsequent experiments were focused on homozygous mutant (*Grb10Δ2-4^{m/p}*) animals that displayed the most pronounced change in their ability to clear glucose. To investigate whether the altered glucose tolerance seen for *Grb10Δ2-4^{m/p}* mice might be detected in younger animals, an additional experiment was conducted with a cohort of male mice 18 to 22 weeks of age (Fig. 4C). Again, these animals exhibited a significant improvement in the ability to clear a glucose load compared with weight-matched wild-type males (*P* < 0.001). To investigate the mechanism for the enhanced glucose clearance, levels of serum insulin were also measured during the GTT. These were slightly lower in *Grb10Δ2-4^{m/p}* males (Fig. 4D), consistent with the serum insulin concentration being reduced, though not significantly so, in older *Grb10Δ2-4^{m/+}* animals that had been fed ad libitum (Fig. 3B). Thus, the improved glucose tolerance could not be attributed to increased insulin levels.

To determine the role of individual tissues in the improved

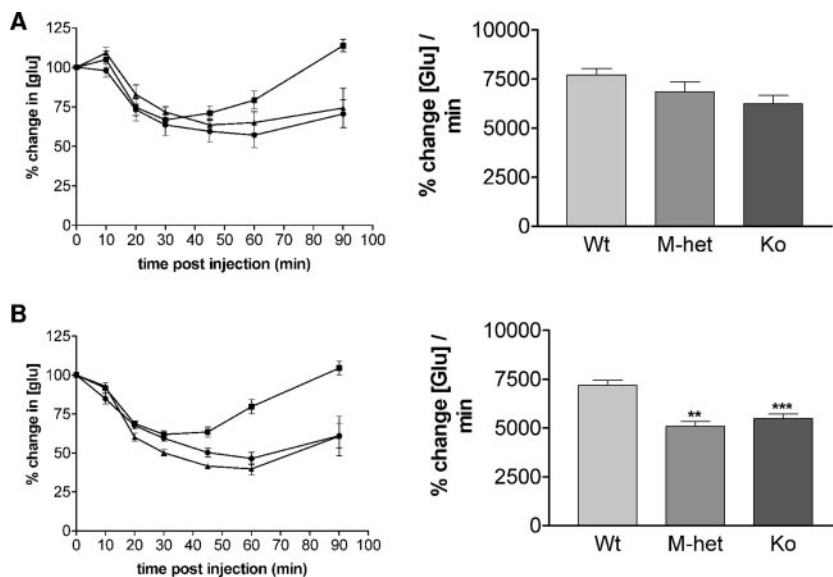


FIG. 6. Improved insulin action in *Grb10Δ2-4* mutant mice. Results of i.p. ITT for male (A) and female (B) mice at 17 to 21 weeks of age who fasted overnight (left panels) are shown, with *Grb10Δ2-4^{m/+}* (M-het), and *Grb10Δ2-4^{m/p}* (Ko) animals compared to wild-type (Wt) controls. The incremental areas under the glucose curves are shown (right panels). All results are expressed as means ± SEM (**, *P* < 0.05; ***, *P* < 0.001 [ANOVA]).

glucose tolerance, further tests were performed with adult male *Grb10Δ2-4^{m/p}* animals and controls, with the glucose load labeled with trace amounts of 2-[³H]DOG (Fig. 5A) and [U-¹⁴C]glucose (Fig. 5B). Clearances of 2-[³H]DOG into quadriceps muscle and brown adipose tissue were very similar between the two genotypes, and although *Grb10Δ2-4^{m/p}* animals showed a modest increase in uptake to tibialis muscle and WAT, these changes were not statistically significant. Nonsignificant trends for an increase in [U-¹⁴C]glucose incorporation into glycogen in quadriceps and tibialis muscle and into lipid in WAT were observed for *Grb10Δ2-4^{m/p}* animals. However, incorporation into liver glycogen was significantly decreased, possibly reflecting clearance into the increased muscle mass of these mice (Fig. 2).

To test whether increased insulin sensitivity might contribute to the improved ability to clear a glucose load, we performed i.p. ITTs on mice at 17 to 21 weeks of age (Fig. 6). A trend towards increased insulin sensitivity was seen for both *Grb10Δ2-4^{m/+}* and *Grb10Δ2-4^{m/p}* males (Fig. 6A). In the case of females, both *Grb10Δ2-4^{m/+}* and *Grb10Δ2-4^{m/p}* genotypes exhibited a significant enhancement in the ability of insulin to lower blood glucose levels (Fig. 6B). Similar results were obtained when younger (8- to 12-week-old) males and females were tested, suggesting that the increased insulin sensitivity is not strongly influenced by age (data not shown).

Insr signaling in skeletal muscle and WAT. Conflicting data regarding the regulatory role of Grb10 in Insr signal transduction have been published (27). Therefore, we sought to establish whether changes occur in the insulin signaling pathway in *Grb10Δ2-4* mutant animals. We focused on skeletal muscle (Fig. 7) and WAT (Fig. 8), as they are the two major insulin-responsive tissues that are sites of Grb10 expression in adult mice (Fig. 1). Cell lysates were prepared from tissues isolated from control and insulin-stimulated adult male mice. Western blot analysis revealed that *Grb10Δ2-4^{m/p}* mouse samples exhibited a significant increase in the total amount of Insr, both in skeletal muscle (Fig. 7A) and in WAT (Fig. 8A). In order to establish an *in vivo* interaction between Grb10 and the Insr, coimmunoprecipitations were carried out on skeletal muscle samples using an anti-Insr antibody, followed by Western blotting with an anti-Grb10 antibody (Fig. 7B). Comparing samples from wild-type and *Grb10Δ2-4^{m/+}* animals, we detected Grb10 protein in the wild-type samples but not in the *Grb10* mutant tissue, as expected. To determine whether Grb10 disruption altered tyrosine phosphorylation of the Insr, lysates were immunoprecipitated with an anti-Insr antibody and Western blotted with two different anti-phosphotyrosine-specific antibodies. The first antibody was specific to phosphotyrosines 1162/1163 (pY1162/3) within the activation loop of the Insr. This revealed a significant decrease in insulin-stimulated receptor phosphorylation in skeletal muscle (Fig. 7C and D) and a marked reduction in WAT (Fig. 8B and C). The other antibody used (pY4G10) does not discriminate between Insr phosphotyrosine residues, and it also revealed a trend towards reduced insulin-stimulated Insr phosphorylation in *Grb10Δ2-4^{m/p}* samples in both skeletal muscle (Fig. 7C and E) and WAT (Fig. 8B and D), although in both cases, this did not reach statistical significance. Taken together, these data suggest that Grb10 protects the Insr from activation loop dephosphorylation by specific PTPs in a manner similar to that recently

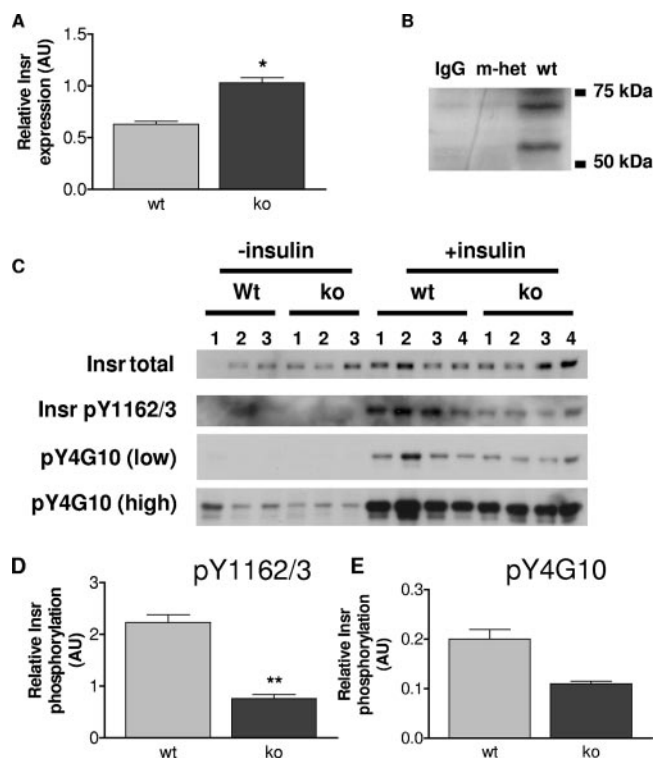


FIG. 7. Insr levels and tyrosine phosphorylation in quadriceps muscles from wild-type (wt) and *Grb10Δ2-4^{m/p}* (ko) mice. AU, arbitrary units. (A) Insr levels in the absence of insulin treatment. Tissue lysates were Western blotted with antibodies that recognize all forms of the Insr. Following densitometric analysis, total Insr levels were normalized using total extracellular signal-regulated kinase as a loading control. (B) Coimmunoprecipitation of Grb10 with the Insr. Bands of the expected size for Grb10 (located between markers at 50 kDa and 75 kDa) were detected in skeletal muscle samples from wild-type animals (wt) but not *Grb10Δ2-4^{m/+}* animals (m-het) following immunoprecipitation with an anti-Insr antibody and then Western blotting with an anti-Grb10 antibody. Similarly, no Grb10 protein was detected when the anti-Insr antibody was omitted from the immunoprecipitation reaction (immunoglobulin G control [IgG]). (C) Insr tyrosine phosphorylation. Following immunoprecipitation of the Insr, Western blots were probed with antibodies that recognize either Insr phosphorylated within the activation loop (pY1162/3) or all tyrosine-phosphorylated forms of the Insr (pY4G10). Both low and high exposures of the same blot are shown for the pY4G10 antibody. Immunoprecipitates were also Western blotted for total Insr content. (D) Insr phosphorylation within the activation loop, normalized for total Insr levels. (E) Levels of all tyrosine-phosphorylated forms of Insr, normalized for total Insr levels. All results are expressed as means \pm SEM (*, $P < 0.05$; **, $P < 0.01$ [Student's *t* test]).

reported for Grb14 (15, 46). Consistent with this, analysis of Insr immunoprecipitates from WAT for tyrosine phosphorylation at a site outside of the activation loop, pY972, showed no difference between wild-type and *Grb10Δ2-4^{m/p}* mouse samples (Fig. 8E).

Tyrosine-612 phosphorylation of IRS-1 leads to binding of the p85 subunit of PI3K and subsequent activation of Akt, key events in insulin-induced signaling (reviewed in reference 51). To further investigate the possibility of altered signaling in this pathway, tissue lysates from insulin-treated animals were Western blotted with an antibody that recognizes this phosphorylation site as well as an antibody against total IRS-1 (Fig.

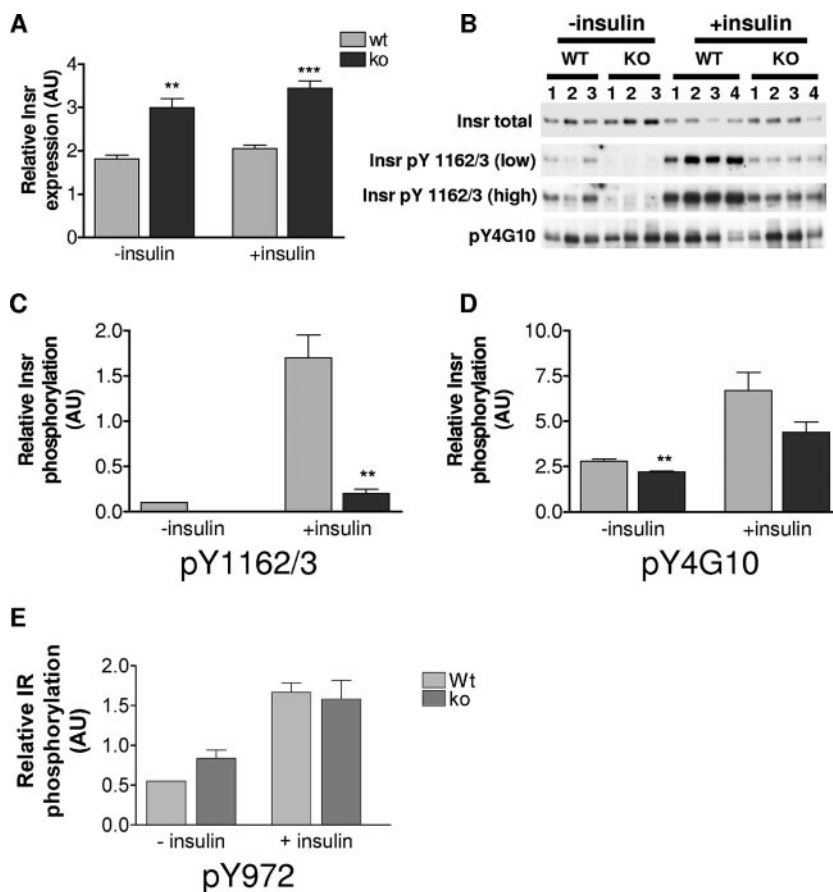


FIG. 8. Insr levels and tyrosine phosphorylation in WAT from wild-type (wt) and *Grb10* $\Delta 2-4^{m/p}$ (ko) mice. AU, arbitrary units. (A) Insr levels. These were determined as described for Fig. 7A. (B) Insr tyrosine phosphorylation from control (–insulin) and insulin-stimulated (+insulin) animals was determined as described for Fig. 7C. Both low and high exposures of the same blot are shown for the pY1162/3 antibody. (C) Insr phosphorylation within the activation loop (Y1162/3), normalized for total Insr levels. (D) Levels of all tyrosine phosphorylated forms of Insr (pY4G10), normalized for total Insr levels. (E) Insr phosphorylation within the region that acts as a docking site for IRS-1 (pY972), normalized for total Insr levels. All results are expressed as means \pm SEM (**, $P < 0.01$; ***, $P < 0.001$ [Student's t test]).

9A). Phosphorylated IRS-1 was significantly increased in the quadriceps muscle samples of *Grb10* $\Delta 2-4^{m/p}$ mice, and the difference appeared more pronounced when corrected for the total amount of IRS-1 present in each sample (Fig. 9B). *Grb10* $\Delta 2-4^{m/p}$ samples showed a significant increase in the level of phosphorylated IRS-1, though only after correcting for the totals amount of IRS-1 present, in both tibialis muscle (Fig. 9C) and WAT (Fig. 9D).

Finally, we determined Akt activation in the same cell lysates by Western blotting with an antibody recognizing Akt phosphorylated at serine 473 (Fig. 10A). Interestingly, relative Akt activation was significantly higher in quadriceps muscles (Fig. 10B) and tibialis muscles (Fig. 10C) from *Grb10* $\Delta 2-4^{m/p}$ animals but only in the basal state and not in samples from insulin-treated animals. In WAT, the level of phosphorylated Akt was reduced in *Grb10* $\Delta 2-4^{m/p}$ samples, though this was statistically significant only in samples from insulin-treated animals (Fig. 10D). Consequently, at the dose of insulin and time point examined, the enhanced insulin-induced IRS-1 phosphorylation observed in muscle and adipose tissue of *Grb10* $\Delta 2-4$ mutant animals is not paralleled by a corresponding increase in Akt activation.

Igf1r signaling in skeletal muscle. Several studies indicate that *Grb10* may act as a negative regulator of Igf1r as well as Insr signaling. Since Igf1r signaling might contribute to either the growth or metabolic effects seen in *Grb10* $\Delta 2-4$ mutant mice, we examined Igf1r signaling in skeletal muscles at the level of the receptor and downstream signaling components (Fig. 11). As expected, mice injected with a bolus of IGF1 demonstrated a marked increase in phosphorylation of Igf1r, IRS-1, and Akt. Compared with lysates from wild-type animals, lysates from the *Grb10* $\Delta 2-4^{m/p}$ mice were found to have a modest (10 to 20%) increase in Igf1r levels and, at the same time, a reduction in tyrosine phosphorylation within the activation loop (Y1162/3). Densitometric analysis revealed that Y1162/3 phosphorylation was reduced by approximately twofold in quadriceps muscles and to a lesser extent in tibialis muscles. Associated with the receptor hypophosphorylation, tyrosine phosphorylation of IRS-1 was increased approximately twofold in both muscle types, but this did not result in a change in the level of Akt phosphorylation. The effects on IGF1-stimulated Igf1r signaling were therefore analogous to those observed at the Insr following stimulation with insulin.

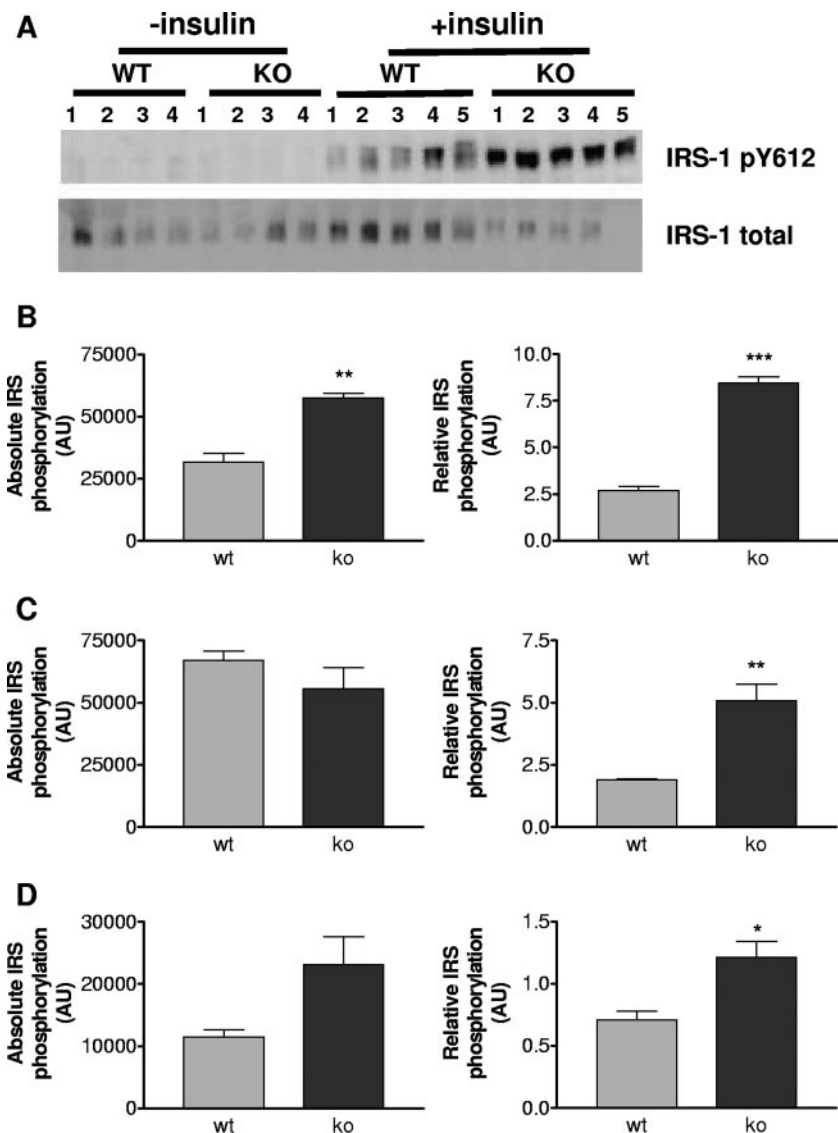


FIG. 9. IRS-1 tyrosine phosphorylation in wild-type (wt) and *Grb10* Δ 2-4^{m/p} (ko) mice. (A) Tissue lysates from both control (–insulin) and insulin-stimulated (+insulin) animals were Western blotted with antibodies specific for Y612-phosphorylated IRS-1 and for total IRS-1. Blots of quadriceps muscle lysates are shown as an example. (B to D) Absolute levels of insulin-stimulated IRS-1 tyrosine phosphorylation (left panels) and relative levels of tyrosine-phosphorylated IRS-1 (that have been corrected for total IRS-1) (right panels) in quadriceps muscle (B), tibialis muscle (C), and WAT (D) are shown. All results are expressed as means \pm SEM (*, $P < 0.05$; **, $P < 0.01$; ***, $P < 0.001$ [Student's *t* test]). AU, arbitrary units.

DISCUSSION

The Grb10 adapter protein is capable of interacting strongly with the Insr, and a number of biochemical studies provide evidence that it may act to modulate Insr signaling (reviewed in references 27 and 36). Most of these studies have involved the expression of exogenous Grb10 in cultured cells, and the majority support a model in which Grb10 acts to inhibit Insr signaling, although evidence to the contrary has been presented (27). Here, in order to gain an insight into the physiological role of this protein, we examined mice with a disrupted *Grb10* gene for evidence of changes in glucose metabolism and Insr signaling.

The mutant *Grb10* Δ 2-4 allele includes the replacement of three exons, including the first two protein-coding exons, with

a *LacZ* reporter gene (12). We have previously shown that expression from the *LacZ* reporter gene closely follows the endogenous pattern of *Grb10* expression, as determined by mRNA in situ hybridization. During embryogenesis, *Grb10* expression was widespread in tissues of mesodermal and endodermal origins, and this expression was predominantly from the maternal allele, confirming that *Grb10* is subject to regulation by genomic imprinting. In this study, we found *Grb10* expression in adult mice to be restricted to fewer tissues, including, notably, both canonical (skeletal muscle and WAT) and noncanonical (islets of Langerhans and hypothalamus) insulin-responsive tissues. These sites of expression were consistent with previous reports of *Grb10* expression in rodents. Northern blots of mRNA from adult mouse tissues have shown

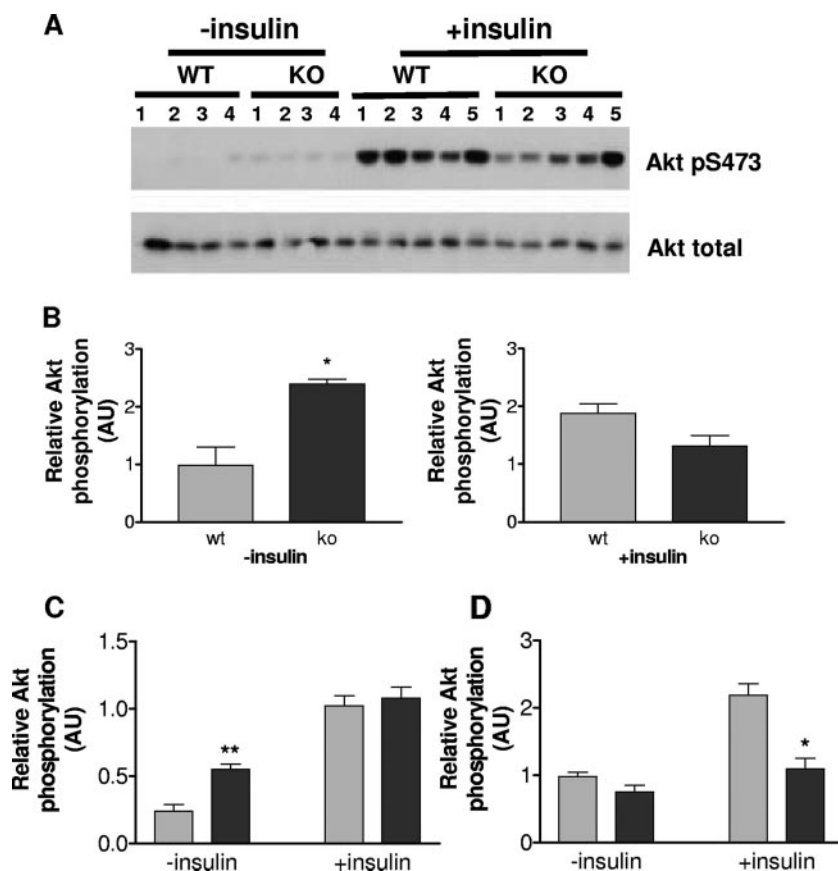


FIG. 10. Akt activation in wild-type (wt) and *Grb10* $\Delta 2-4^{m/p}$ (ko) mice. AU, arbitrary units. (A) Tissue lysates from both control and insulin-stimulated animals were Western blotted with antibodies specific for Akt phosphorylated at serine 473 (Akt pS473) and for total Akt. Blots of quadriceps muscle lysates are shown as an example. Results for control (–insulin) and insulin-stimulated (+insulin) samples were scanned for densitometry following exposure to film for different lengths of time and are consequently displayed on separate histograms. (B to D) Relative levels of serine 473-phosphorylated Akt, corrected for total Akt levels in quadriceps muscle (B), tibialis muscle (C), and WAT (D) are shown. All results are expressed as means \pm SEM (*, $P < 0.05$; **, $P < 0.01$ [Student's t test]).

high levels of *Grb10* expression in skeletal muscles, WAT, hearts, and kidneys, with lower levels in brains, lungs, and testes (34, 47). No *LacZ* expression was detected in livers of adult *Grb10* $\Delta 2-4$ animals, which is consistent with both Northern analyses of mice (36, 47) and a reverse transcription-PCR study showing extinction of *Grb10* expression in the liver of the postnatal rat (22). Use of the *Grb10* $\Delta 2-4$ mutant mice allowed us to evaluate allele-specific expression following either maternal or paternal transmission of the *LacZ*-tagged allele. At most sites of expression, β -galactosidase activity was detected only from the maternal allele, demonstrating that imprinting of *Grb10* is maintained into adulthood. The exception was the hypothalamus, in which *Grb10* expression was exclusively from the paternal allele, establishing that *Grb10* is oppositely imprinted in this tissue. Interestingly, expression from the paternal allele within the central nervous system also appears to be established during embryogenesis (A. S. Garfield and A. Ward, unpublished data) and is consistent with recently characterized brain-specific *Grb10* transcripts that may be under the control of a putative regulatory element that is hypomethylated on the paternal allele in the brain (2, 26).

We next evaluated the body mass and composition of adult *Grb10* $\Delta 2-4$ mutant mice. At 6 months of age, both

male and female *Grb10* $\Delta 2-4^{m/+}$ animals were approximately 13% heavier than wild-type littermates. This outcome compares with mean birth weights of *Grb10* $\Delta 2-4^{m/+}$ animals being approximately 36% greater than normal (see reference 12). Thus, the increased body mass of *Grb10* $\Delta 2-4^{m/+}$ animals persisted into adulthood, but the weight differential was, for both sexes, less than that observed on the day of birth. DXA measurements revealed that *Grb10* $\Delta 2-4^{m/+}$ adults retain larger bodies and have altered body compositions, with increased lean tissue contents and reduced amounts of adipose, suggesting that the narrowing of the difference in body mass can, at least in part, be accounted for by reduced adiposity in *Grb10* $\Delta 2-4^{m/+}$ animals. In support of this hypothesis, weight was monitored from birth to 80 days of age, for one cohort of animals, showing that the weight difference diminished mainly during the postweaning period. Furthermore, levels of the hormone leptin were reduced in sera from *Grb10* $\Delta 2-4^{m/+}$ animals in proportion with the reduced WAT mass, consistent with the established correlation between leptin concentration and adipose tissue mass (20). However, while leptin levels could be correlated with body mass for wild-type animals (i.e., heavier wild types result from excess adipose deposition), there was no significant correlation for *Grb10* $\Delta 2-4^{m/+}$ mice, leading to the

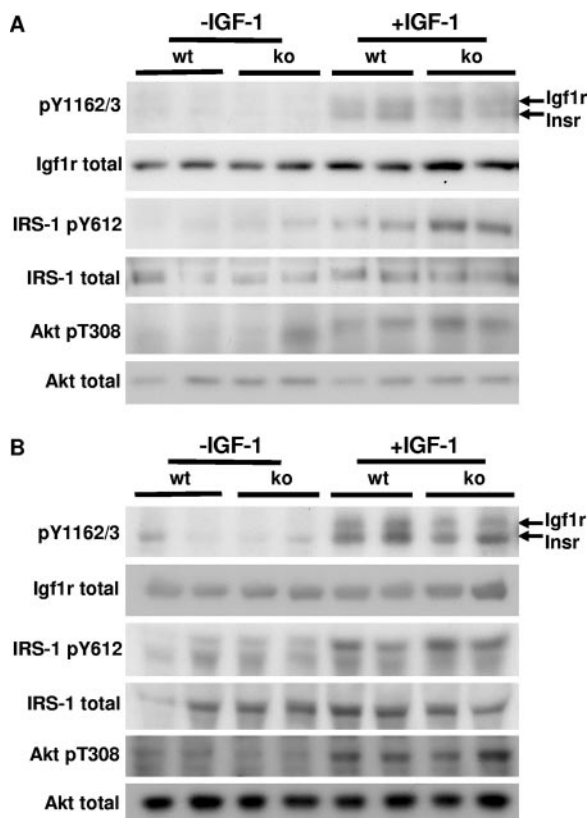


FIG. 11. IGF1R signaling in skeletal muscles of wild-type (wt) and *Grb10Δ2-4^{m/p}* (ko) mice. Tissue lysates from tibialis (A) and quadriceps (B) muscles were prepared from animals injected with IGF1 (+IGF-1) and control animals injected with vehicle alone (-IGF-1). Lysates were Western blotted directly with antibodies that recognize all forms of Igf1r (Igf1r total), Igf1r phosphorylated within the activation loop (pY1162/3; note that this antibody also detects the equivalent phosphorylated Insr isoforms), total IRS-1, tyrosine-phosphorylated IRS-1 (IRS-1 pY612), total Akt, or threonine-phosphorylated Akt (Akt T308).

inference that, in this case, lean mass is the major contributing factor to variability in body size. Loss of the relationship between plasma leptin and body weight has been reported in studies using other models of mice with reduced adiposity, and in some cases, there is an associated reduction in the mean size of adipocytes (e.g., see references 6 and 32). This was not obviously the case for *Grb10Δ2-4^{m/+}* mice, as histological analysis of gonadal WAT showed no difference between the sizes of the adipocytes of the *Grb10Δ2-4^{m/+}* mice and those of the wild-type littermate controls. Measurements of food intake indicated that the lean phenotype was not associated with hypophagia and, despite reduced serum leptin levels, *Grb10Δ2-4* mutant mice ate appropriately for their body weight. Similar observations have been made in studies of myostatin gene (*Mstn*, also known as *Gdf8*) KO mice that also have increased lean body mass, in this case, due to a combination of increased skeletal muscle hypertrophy and hyperplasia (37, 41). This suggests that for both *Grb10* and *Mstn* mutants, central sensitivity to leptin has been improved or the reduction in the leptin level has been compensated, perhaps

through increased sensitivity to the antiorexigenic effects of insulin.

To investigate whether energy metabolism might be altered, mice 6 to 10 months of age were subjected to standard GTT, revealing that both *Grb10Δ2-4^{m/+}* and *Grb10Δ2-4^{m/p}* males and also *Grb10Δ2-4^{m/p}* females had a significantly improved ability to clear a glucose load. The observation that the effects seen in *Grb10Δ2-4^{m/p}* mice were more pronounced than those in *Grb10Δ2-4^{m/+}* mice is likely to reflect the fact that although fetal *Grb10* expression occurs predominantly from the maternal allele, there was some expression from the paternal allele (12). Alternatively, expression that we observed from the paternal *Grb10* allele in the hypothalamus might contribute to the improved glucose homeostasis. A role for *Grb10* in the hypothalamus has yet to be established; however, mice with a brain-specific KO of *Insr* were shown to have altered glucose homeostasis, including increased susceptibility to diet-induced obesity and mild insulin resistance (7), while mice with a brain-specific disruption of PTP-1B, known as a negative regulator of *Insr* signaling, had a contrasting phenotype, with reduced adiposity and improved sensitivity to both insulin and glucose (4). Trends for lower serum insulin levels in 18- to 22-week-old *Grb10Δ2-4^{m/p}* mice during a GTT clearly demonstrated that the improved glucose tolerance was not the result of enhanced insulin release in response to the glucose load and suggested enhanced insulin action. This conclusion was confirmed by the results of ITT, for which *Grb10Δ2-4^{m/p}* animals displayed a reduction in serum glucose levels greater than that displayed by wild-type controls, following the same challenge with exogenous insulin. To assess the role of different insulin-responsive tissues in the altered metabolic phenotype, we performed GTT for which the glucose load was labeled with trace amounts of 2-[³H]DOG and [U-¹⁴C]glucose. Although these experiments showed no significant differences in the clearance of 2-[³H]DOG or [U-¹⁴C]glucose into insulin-sensitive tissues per gram of fresh weight, there was a trend towards greater uptake of both labels into skeletal muscles and WAT in *Grb10Δ2-4^{m/p}* animals. The greater mass of muscles in *Grb10Δ2-4^{m/p}* mice indicates that on a whole-body basis, the improved glucose tolerance most likely results from increased glucose clearance into muscle. At the same time, *Grb10Δ2-4^{m/p}* animals incorporated significantly less [U-¹⁴C]glucose into glycogen in the liver, a result which probably also reflects disposal of a larger portion of the glucose load into muscle tissue.

The availability of *Grb10Δ2-4* mutant mice has allowed us to determine, for the first time, the role of *Grb10* in insulin signaling in a physiological context. Coimmunoprecipitation experiments indicated that *Grb10* may interact directly with the *Insr* in vivo. Additionally, several changes occurred at the *Insr*/IRS-1 node of the insulin signaling network in *Grb10Δ2-4^{m/p}* animals. In both quadriceps muscles and WAT from *Grb10Δ2-4^{m/p}* mice, there was a modest but significant increase in *Insr* expression levels. This finding is consistent with evidence that *Grb10* promotes the ubiquitin-targeted degradation of the Igf1r (59) and *Insr* (50). However, a marked reduction in receptor phosphorylation was detected in quadriceps muscles and WAT from *Grb10Δ2-4^{m/p}* mice when an antibody specific for tyrosine phosphorylation within the activation loop (pY1162/3) was used. In contrast to the case with *Grb14*-deficient mice (15), this effect was not observed in the liver (data not shown),

consistent with expression of Grb14, but not Grb10, in this organ. Only a modest reduction in the level of phosphorylated receptor was observed for *Grb10Δ2-4^{m/p}* animals when an antibody that recognizes all tyrosine-phosphorylated forms of the Insr was used, suggesting that Grb10 preferentially protects the activation loop phosphotyrosines. This interpretation was supported by measurement of tyrosine phosphorylation at Y972, a site located near the Insr transmembrane domain that is thought to be involved in the docking of substrates such as IRS-1 and Shc (14). In contrast to the dramatic reduction in tyrosine phosphorylation seen within the activation loop, there was no significant change in pY972 phosphorylation in *Grb10Δ2-4^{m/p}* tissue samples. Our data are therefore consistent with the recent study of Nouaille et al. (46), which determined that Grb14 protects the three tyrosines within the activation loop (Y1158, Y1162, and Y1163) from dephosphorylation by PTP-1B while at the same time favoring dephosphorylation of Y972. A model for interaction of Grb14 with the Insr based on the Insr/Grb14 BPS domain, Insr/APS SH2 domain, and Grb14 SH2 domain crystal structures provides a mechanistic basis for this, since pY1158 and pY1162 are engaged by the Grb14 SH2 domain, while pY1163 interacts with the BPS region (17). This model may also apply to binding of Grb10 to the Insr, since the key interacting residues are conserved between Grb10 and Grb14. Furthermore, this regulatory role of Grb10 may extend to the closely related Igf1r, since we observed a reduction in pY1162/3 phosphorylation in skeletal muscle from *Grb10Δ2-4^{m/p}* mice, compared to wild-type animals, following IGF1 stimulation in vivo. Similarly, suppression of Grb10 by RNA interference resulted in hypophosphorylation of Igf1r Y1158 in IGF1-stimulated cells (18).

Despite the decrease in activation loop phosphorylation in skeletal muscle and WAT of *Grb10Δ2-4^{m/p}* mice, relative tyrosine phosphorylation of IRS-1 in these mice was significantly greater than that in wild-type controls. Enhancement of IRS-1 tyrosine phosphorylation was particularly marked in the quadriceps muscle. Contrasting effects on receptor and IRS-1 phosphorylation were also observed in Grb14-deficient livers following insulin stimulation (15) and in NIH 3T3 cells subjected to *Grb10* knockdown followed by IGF1 treatment (18). A potential explanation for this apparent paradox is spatial segregation of signaling events. Dephosphorylation of the Insr by PTP-1B is thought to occur following receptor internalization into endosomes (3). If, in the absence of Grb10, dephosphorylation of Insr occurs predominantly in the endosomal compartment, then tyrosine phosphorylation of IRS-1, which occurs at the plasma membrane (11), could still be enhanced due to loss of pseudosubstrate inhibition of the Insr (17) or increased Insr/IRS coupling due to the lack of steric repression by Grb10 (63). Furthermore, our observation that insulin-stimulated pY972 phosphorylation is essentially unaltered in Grb10-deficient mice suggests that Grb10 functions in a manner similar to that of Grb14 and regulates site-specific phosphorylation of the Insr (46). It is possible that in the absence of Grb10, the residual phosphorylated (predominantly at pY972) receptor has increased catalytic activity, due to loss of pseudosubstrate inhibition, that leads to enhanced IRS-1 activation. Alternatively, prolonged association of the Insr with IRS-1 could affect the susceptibility of IRS-1 to specific phosphatases. Overall, these data highlight Grb10 as an important

physiological regulator of insulin-induced Insr and IRS-1 tyrosine phosphorylation. Also of note is that Grb10, like Grb14, performs this role in a tissue-specific manner. Thus, while both Grb10 and Grb14 regulate insulin signaling in skeletal muscle, only *Grb14* gene disruption affects Insr and IRS-1 phosphorylation in liver and only Grb10 affects these end points in WAT (as shown in reference 15, this study, and data not shown). These findings are consistent with the expression profiles of the two adaptor proteins, with Grb14 expression highest in liver, lower in WAT, and lowest in muscle (9), while Grb10 expression is relatively high in skeletal muscle and WAT but absent from liver (see above).

A surprising observation was that the increased insulin-induced IRS-1 phosphorylation in *Grb10Δ2-4^{m/p}* animals was not associated with enhanced Akt activation. This contrasts with the effects of Grb14 ablation (15). However, these data are consistent with the modest effects observed on 2-[³H]DOG uptake and [U-¹⁴C]glucose incorporation into glycogen or lipid in insulin-responsive tissues of *Grb10Δ2-4* mutant mice. Basal Akt activation in the skeletal muscles of *Grb10Δ2-4^{m/p}* mice was significantly higher than that in the skeletal muscles of wild-type mice, while insulin-stimulated activation was essentially unaltered. The increased basal Akt activation was not always supported by elevated IRS-1 phosphorylation and cannot be explained by raised insulin levels. Insulin-induced Akt activation in WAT of the mutant mice was significantly lower than that in WAT of the wild-type mice. One possible explanation for the dissociation of IRS-1 phosphorylation from Akt activation is that the altered body composition of *Grb10Δ2-4^{m/p}* mice results in compensatory negative feedback regulation of PI3K/Akt to avoid excessive glucose uptake by insulin-responsive tissues. For instance, *Grb10Δ2-4^{m/p}* animals could express higher levels of SHIP2 or PTEN. These lipid phosphatases are known to dephosphorylate inositol-3,4,5-trisphosphate, and studies of mice have shown that both act as inhibitors of Akt activity in insulin-responsive tissues (8, 21, 33, 54, 58). An alternative, though not mutually exclusive, explanation is suggested by studies showing that Grb10 can interact directly with the p85 subunit of PI3K (16), and with Akt (28), to enhance the activity of these enzymes. Thus, in the absence of Grb10, activation of PI3K or Akt might be compromised.

Since studies on mouse fibroblasts have identified Grb10 as an endogenous negative regulator of Igf1r signaling (18) and IGF1 acts to increase muscle mass and decrease adipose content (39, 45), a potential explanation for the altered body composition and/or glucose metabolism in Grb10-deficient animals is increased IGF1 signaling in muscle. To test this hypothesis, we administered a bolus of IGF1 to wild-type and *Grb10Δ2-4^{m/p}* mice and assayed signaling events in quadriceps and tibialis muscles. Igf1r levels exhibited a modest increase in *Grb10Δ2-4* mutant mice compared to that in controls. Stimulation of muscle cells with nanomolar concentrations of IGF1 results in tyrosine phosphorylation of both the Igf1r and Insr (52), and this could be detected upon IGF1 administration in vivo, since these receptors exhibit a difference in electrophoretic mobility (34). Densitometric analysis of the relative levels of IGF1-stimulated pY1162/3 activation loop phosphorylation revealed that this was reduced (approximately twofold

in quadriceps muscles and slightly less in tibialis muscles) of *Grb10Δ2-4^{m/p}* animals relative to wild-type controls. At the same time, IGF1-induced IRS-1 tyrosine phosphorylation exhibited an approximately twofold increase in both muscle types of *Grb10*-deficient animals compared to that in the muscles of wild types. Thus, despite reduced Igf1r phosphorylation, IGF1-induced signaling to IRS-1 was enhanced in muscle upon *Grb10* gene disruption. These data are consistent with the effects of small interfering RNA-mediated *Grb10* knockdown in mouse fibroblasts (18). However, the enhanced IRS-1 phosphorylation did not result in increased Akt activation, as determined by T308 phosphorylation. Overall, these experiments indicate that IGF1-induced signaling, at least to IRS-1, is increased in muscles of adult *Grb10*-deficient animals. Postnatal growth is not obviously enhanced in *Grb10*-deficient animals; indeed, the overall size increase in comparison to wild-type littermates diminishes between birth and adulthood, and genetic evidence indicates that *Grb10* regulates fetal growth largely through a non-IGF pathway (12; unpublished data). However, altered Igf1r signaling might contribute to maintenance of increased muscle mass postnatally. The exploration of this possibility will require further characterization of the muscle phenotype and, as appropriate, the signaling pathways regulating muscle hyperplasia and hypertrophy. Of note in this regard, IGF1-induced skeletal muscle hypertrophy is characterized by increased mTOR/p70S6K signaling without increased Akt phosphorylation (56).

Further work will be needed to separate the effects of *Grb10* on body size and proportions, which might have secondary consequences for glucose-regulated metabolism, from any direct physiological effects mediated by its interaction with the *Insr*, or Igf1r, and downstream signaling molecules. Transgenic mice overexpressing *Grb10* during postnatal life were recently shown to exhibit insulin resistance, leading to diabetes in some individuals (53). Thus, the effect of *Grb10* excess on glucose sensitivity mirrored that seen in our *Grb10Δ2-4* mutant mice. The *Grb10* transgenic mice were of normal sizes at birth but as adults had body weights that were reduced by some 10 to 15% compared to the weights of wild-type controls, and their pancreases were reported to have increased adipocyte contents (though it was not clear whether this reflected a more general increase in body fat content). As in *Grb10Δ2-4* mutant mice, these changes in body size and tissue composition could contribute to the altered glucose metabolism, though it is interesting to note that an increase in skeletal muscle alone may not be sufficient to significantly alter blood glucose regulation, since *Mstn* KO mice had unaltered serum glucose and insulin levels (fed or fasting) and responded normally to GTT (41).

Mouse gene KO studies have established that several factors known to interact directly with the *Insr* can each have a significant influence over the systemic regulation of glucose levels. It is striking that *Grb10Δ2-4* mutant mice share phenotypic features with mice lacking either PTP-1B (19, 32) or the signaling adaptor proteins APS (42) and *Grb14* (15), including enhanced *Insr* signaling (PTP-1B and *Grb14*) and improved glucose tolerance (all three KO models), despite reduced levels of circulating insulin. Each of these factors could be considered a potential therapeutic target for improved insulin action, with the possibility that the targeting

of specific molecules might allow differential modulation of *Insr* signaling in different tissues (for instance, enhanced *Insr* signaling in adipose tissue of *Grb10* KO mice but not PTP-1B KO, *Grb14* KO, or APS KO mice) and with potentially different physiological outcomes (e.g., *Grb10* KO and PTP-1B KO mice were found to be lean, whereas adiposity was unaltered in *Grb14* KO and APS KO mice). These differences might, in part, be due to overlapping functions, particularly between the three adaptor proteins, that may differ at the level of individual tissues.

Epidemiological studies have demonstrated a relationship between restricted fetal growth and an increased susceptibility to insulin resistance, obesity, and type 2 diabetes, as well as other features of the metabolic syndrome in adulthood. This phenomenon of fetal programming has been modeled in animals, typically by using dietary restriction during pregnancy (23, 48, 49). The underlying mechanism has not been determined but is likely to have an epigenetic basis. Indeed, recent studies of mice have shown that manipulations of the diet during pregnancy can affect patterns of DNA methylation in the offspring (61, 62). Affected genes include at least some of those that are imprinted. This study, together with our previous report (12), indicates that *Grb10* forms a link between fetal growth regulation and adult metabolic health status, a result which, together with the imprinted nature of the *Grb10* gene, suggests *Grb10* as a candidate for involvement in the fetal-programming phenomenon.

ACKNOWLEDGMENTS

We thank Iryna Withington, Tracey Crew, and 5WL1 staff for technical assistance and members of the Ward and Daly laboratories for stimulating discussions.

The work was funded by the Biotechnology and Biological Sciences Research Council and the Medical Research Council (United Kingdom) and by the National Health and Medical Research Council of Australia. F.M.S. was funded in part by a CASE award sponsored by GlaxoSmithKline.

REFERENCES

- Accili, D., J. Drago, E. J. Lee, M. D. Johnson, M. H. Cool, P. Salvatore, L. D. Asico, P. A. Jose, S. I. Taylor, and H. Westphal. 1996. Early neonatal death in mice homozygous for a null allele of the insulin receptor gene. *Nat. Genet.* **12**:106–109.
- Arnaud, P., D. Monk, M. Hitchins, E. Gordon, W. Dean, C. V. Beechey, J. Peters, W. Craigen, M. Preece, P. Stanier, G. E. Moore, and G. Kelsey. 2003. Conserved methylation imprints in the human and mouse *GRB10* genes with divergent allelic expression suggests differential reading of the same mark. *Hum. Mol. Genet.* **12**:1005–1019.
- Asante-Appiah, E., and B. P. Kennedy. 2003. Protein tyrosine phosphatases: the quest for negative regulators of insulin action. *Am. J. Physiol. Endocrinol. Metab.* **284**:E663–E670.
- Bence, K. K., M. Delibegovic, B. Xue, C. Z. Gorgun, G. S. Hotamisligil, B. G. Neel, and B. B. Kahn. 2006. Neuronal PTP1B regulates body weight, adiposity and leptin action. *Nat. Med.* **12**:917–924.
- Bennett, W. R., T. E. Crew, J. M. W. Slack, and A. Ward. 2003. Structural-proliferative units and organ growth: effects of insulin-like growth factor 2 on growth of colon and skin. *Development* **130**:1079–1088.
- Blucher, M., M. D. Michael, O. D. Peroni, K. Ueki, N. Carter, B. B. Kahn, and C. R. Kahn. 2002. Adipose tissue selective insulin receptor knockout protects against obesity and obesity-related glucose intolerance. *Dev. Cell* **3**:25–38.
- Bruning, J. C., D. Gautam, D. J. Burks, J. Gillette, M. Schubert, P. C. Orban, R. Klein, W. Krone, D. Muller-Wieland, and C. R. Kahn. 2000. Role of brain insulin receptor in control of body weight and reproduction. *Science* **289**:2122–2125.
- Butler, M., R. A. McKay, I. J. Popoff, W. A. Gaarde, D. Witchell, S. F. Murray, N. M. Dean, S. Bhanot, and B. P. Monia. 2002. Specific inhibition of PTEN expression reverses hyperglycemia in diabetic mice. *Diabetes* **51**:1028–1034.
- Cariou, B., N. Capitaine, V. Le Marcis, N. Vega, V. Bereziat, M. Kergoat, M.

- Laville, J. Girard, H. Vidal, and A. F. Burnol. 2004. Increased adipose tissue expression of Grb14 in several models of insulin resistance. *FASEB J.* **18**: 965–967.
10. Cariou, B., D. Perdureau, K. Cailliau, E. Browaeys-Poly, V. Berezat, M. Vasseur-Cognet, J. Girard, and A. F. Burnol. 2002. The adapter protein ZIP binds Grb14 and regulates its inhibitory action on insulin signaling by recruiting protein kinase C ζ . *Mol. Cell. Biol.* **22**:6959–6970.
 11. Ceresa, B. P., A. W. Kao, S. R. Santeler, and J. E. Pessin. 1998. Inhibition of clathrin-mediated endocytosis selectively attenuates specific insulin receptor signal transduction pathways. *Mol. Cell. Biol.* **18**:3862–3870.
 12. Charalambous, M., F. M. Smith, W. R. Bennett, T. E. Crew, F. Mackenzie, and A. Ward. 2003. Disruption of the imprinted *Grb10* gene leads to disproportionate overgrowth by an *Igf2* independent mechanism. *Proc. Natl. Acad. Sci. USA* **100**:8292–8297.
 13. Charalambous, M., A. Ward, and L. D. Hurst. 2003. Evidence for a priming effect on maternal resource allocation: implications for interbrood competition. *Proc. R. Soc. Biol. Sci. Ser. B* **270**:S100–S103.
 14. Combettes-Souverein, M., and T. Issad. 1998. Molecular basis of insulin action. *Diabetes Metab.* **24**:477–489.
 15. Cooney, G., R. J. Lyons, A. J. Crew, T. E. Jensen, J. C. Molero, C. J. Mitchell, T. J. Biden, C. J. Ormandy, D. E. James, and R. J. Daly. 2004. Improved glucose homeostasis and enhanced insulin signalling in Grb14-deficient mice. *EMBO J.* **23**:582–593.
 16. Deng, Y., S. Bhattacharya, O. R. Swamy, R. Tandon, Y. Wang, R. Janda, and H. Riedel. 2003. Growth factor receptor-binding protein 10 (Grb10) as a partner of phosphatidylinositol 3-kinase in metabolic insulin action. *J. Biol. Chem.* **278**:39311–39322.
 17. Depetris, R. S., J. Hu, I. Gimpelevich, L. J. Holt, R. J. Daly, and S. R. Hubbard. 2005. Structural basis for inhibition of the insulin receptor by the adaptor protein Grb14. *Mol. Cell* **20**:325–333.
 18. Dufresne, A. M., and R. J. Smith. 2005. The adapter protein GRB10 is an endogenous negative regulator of insulin-like growth factor signaling. *Endocrinology* **146**:4399–4409.
 19. Elchebly, M., P. Payette, E. Michaliszyn, W. Cromlish, S. Collins, A. L. Loy, D. Normandin, A. Cheng, J. Himms-Hagen, C.-C. Chan, C. Ramachandran, M. J. Gresser, M. L. Tremblay, and B. P. Kennedy. 1999. Increased insulin sensitivity and obesity resistance in mice lacking the protein tyrosine phosphatase-1B gene. *Science* **283**:1544–1548.
 20. Friedman, J. M., and J. L. Halaas. 1998. Leptin and the regulation of body weight in mammals. *Nature* **395**:763–770.
 21. Fukui, K., T. Wada, S. Kagawa, K. Nagira, M. Ikubo, H. Ishihara, M. Kobayashi, and T. Sasaoka. 2005. Impact of the liver-specific expression of SHIP2 (SH2-containing inositol 5'-phosphatase 2) on insulin signaling and glucose metabolism in mice. *Diabetes* **54**:1958–1967.
 22. Gruppiso, P. A., J. M. Boylan, and C. A. Vaslet. 2000. Identification of candidate growth-regulating genes that are overexpressed in late gestation fetal liver in the rat. *Biochim. Biophys. Acta* **1494**:242–247.
 23. Hales, C. N., and S. E. Ozanne. 2003. For debate: fetal and early postnatal growth restriction lead to diabetes, the metabolic syndrome and renal failure. *Diabetologia* **46**:1013–1019.
 24. Han, D. C., T.-L. Shen, and J.-L. Guan. 2001. The Grb7 family proteins: structure, interactions with other signalling molecules and potential cellular functions. *Oncogene* **20**:6315–6321.
 25. He, W., D. W. Rose, J. M. Olefsky, and T. A. Gustafson. 1998. Grb10 interacts differentially with the insulin receptor, insulin-like growth factor I receptor, and epidermal growth factor receptor via the Grb10 Src homology 2 (SH2) domain and a second novel domain located between the pleckstrin homology and SH2 domains. *J. Biol. Chem.* **273**:6860–6867.
 26. Hikichi, T., T. Kohda, T. Kaneko-Ishino, and F. Ishino. 2003. Imprinting regulation of the murine *Meg1/Grb10* and human *GRB10* genes; roles of brain-specific promoters and mouse-specific CTCF-binding sites. *Nucleic Acids Res.* **31**:1398–1406.
 27. Holt, L. J., and K. Siddle. 2005. Grb10 and Grb14: enigmatic regulators of insulin action—and more? *Biochem. J.* **388**:393–406.
 28. Jahn, T., P. Seipel, S. Urschel, C. Peschel, and J. Duyster. 2002. Role for the adaptor protein Grb10 in the activation of Akt. *Mol. Cell. Biol.* **22**:979–991.
 29. Joshi, R. L., B. Lamothe, N. Cordonnier, K. Mesbah, E. Monthieux, J. Jami, and D. Bucchini. 1996. Targeted disruption of the insulin receptor gene in the mouse results in neonatal lethality. *EMBO J.* **15**:1542–1547.
 30. Kasus-Jacobi, A., D. Perdureau, C. Auzan, E. Clauser, E. Van Obberghen, F. Mauvais-Jarvis, J. Girard, and A.-F. Burnol. 1998. Identification of the rat adaptor Grb14 as an inhibitor of insulin actions. *J. Biol. Chem.* **273**:26026–26035.
 31. Kitamura, T., C. R. Kahn, and D. Accili. 2003. Insulin receptor knockout mice. *Annu. Rev. Physiol.* **65**:313–332.
 32. Klamon, L. D., O. Boss, O. D. Peroni, J. K. Kim, J. L. Martino, J. M. Zabolotny, N. Moghal, M. Lubkin, Y. B. Kim, A. H. Sharpe, A. Stricker-Krongrad, G. I. Shulman, B. G. Neel, and B. B. Kahn. 2000. Increased energy expenditure, decreased adiposity, and tissue-specific insulin sensitivity in protein-tyrosine phosphatase 1B-deficient mice. *Mol. Cell. Biol.* **20**: 5479–5489.
 33. Kurlawalla-Martinez, C., B. Stiles, Y. Wang, S. U. Devaskar, B. B. Kahn, and H. Wu. 2005. Insulin hypersensitivity and resistance to streptozotocin-induced diabetes in mice lacking PTEN in adipose tissue. *Mol. Cell. Biol.* **25**:2498–2510.
 34. Laviola, L., F. Giorgino, J. C. Chow, J. A. Baquero, H. Hansen, J. Ooi, J. Zhu, H. Riedel, and R. J. Smith. 1997. The adapter protein Grb10 associates preferentially with the insulin receptor as compared with the IGF-I receptor in mouse fibroblasts. *J. Clin. Investig.* **99**:830–837.
 35. Lee, A. V., S. T. Taylor, J. Greenall, J. D. Mills, D. W. Tonge, P. Zhang, J. George, M. L. Fiorotto, and D. L. Hadsell. 2003. Rapid induction of IGF-IR signaling in normal and tumor tissue following intravenous injection of IGF-I in mice. *Horm. Metab. Res.* **35**:651–655.
 36. Lim, M. A., H. Riedel, and F. Liu. 2004. Grb10: more than a simple adaptor protein. *Front. Biosci.* **9**:387–403.
 37. Lin, J., H. B. Arnold, M. A. Della-Fera, M. J. Azain, D. L. Hartzell, and C. A. Baile. 2002. Myostatin knockout in mice increases myogenesis and decreases adipogenesis. *Biochem. Biophys. Res. Commun.* **291**:701–706.
 38. Liu, F., and R. A. Roth. 1995. Grb-IR: a SH2-domain-containing protein that binds to the insulin receptor and inhibits its function. *Proc. Natl. Acad. Sci. USA* **92**:10287–10291.
 39. Mauras, N., and M. W. Haymond. 2005. Are the metabolic effects of GH and IGF-I separable? *Growth Horm. IGF Res.* **15**:19–27.
 40. McDougall, K. E., M. J. Perry, R. L. Gibson, J. M. Bright, S. M. Colley, J. B. Hodgins, O. Smithies, and J. H. Tobias. 2002. Estrogen-induced osteogenesis in intact female mice lacking ER β . *Am. J. Physiol. Endocrinol. Metab.* **283**:E817–E823.
 41. McPherron, A. C., and S. J. Lee. 2002. Suppression of body fat accumulation in myostatin-deficient mice. *J. Clin. Investig.* **109**:595–601.
 42. Minami, A., M. Iseki, K. Kishi, M. Wang, M. Ogura, N. Furukawa, S. Hayashi, M. Yamada, T. Obata, Y. Takeshita, Y. Nakaya, Y. Bando, K. Izumi, S. A. Moodie, F. Kajiura, M. Matsumoto, K. Takatsu, S. Takaki, and Y. Ebina. 2003. Increased insulin sensitivity and hypoinsulinemia in APS knockout mice. *Diabetes* **52**:2657–2665.
 43. Miyoshi, N., Y. Kuroiwa, T. Kohda, H. Shitara, H. Yonekawa, T. Kawabe, H. Hasegawa, S. C. Barton, M. A. Surani, T. Kaneko-Ishino, and F. Ishino. 1998. Identification of the *Meg1/Grb10* imprinted gene on mouse proximal chromosome 11, a candidate for the Silver-Russell syndrome gene. *Proc. Natl. Acad. Sci. USA* **95**:1102–1107.
 44. Mounier, C., L. Lavoie, V. Dumas, K. Mohammad-Ali, J. Wu, A. Nantel, J. J. M. Bergeron, D. Y. Thomas, and B. I. Posner. 2001. Specific inhibition by hGRB10 ζ of insulin-induced glycogen synthase activation: evidence for a novel signaling pathway. *Mol. Cell. Endocrinol.* **173**:15–27.
 45. Musaro, A., K. McCullagh, A. Paul, L. Houghton, G. Dobrowolny, M. Molinaro, E. R. Barton, H. L. Sweeney, and N. Rosenthal. 2001. Localized *Igf-1* transgene expression sustains hypertrophy and regeneration in senescent skeletal muscle. *Nat. Genet.* **27**:195–200.
 46. Nouaille, S., C. Blanquart, V. Zilberfarb, N. Boute, D. Perdureau, J. Roix, A. F. Burnol, and T. Issad. 2006. Interaction with Grb14 results in site-specific regulation of tyrosine phosphorylation of the insulin receptor. *EMBO Rep.* **7**:512–518.
 47. Ooi, J., V. Yajnik, D. Immanuel, M. Gordon, J. J. Moskow, A. M. Buchberg, and B. Margolis. 1995. The cloning of Grb10 reveals a new family of SH2 domain proteins. *Oncogene* **10**:1621–1630.
 48. Ozanne, S. E., D. Fernandez-Twinn, and C. N. Hales. 2004. Fetal growth and adult diseases. *Semin. Perinatol.* **28**:81–87.
 49. Ozanne, S. E., and C. N. Hales. 2002. Pre- and early postnatal nongenetic determinants of type 2 diabetes. *Expert Rev. Mol. Med.* **2002**:1–14.
 50. Ramos, F. J., P. R. Langlais, D. Hu, L. Q. Dong, and F. Liu. 2006. Grb10 mediates insulin-stimulated degradation of the insulin receptor: a mechanism of negative regulation. *Am. J. Physiol. Endocrinol. Metab.* **290**:E1262–E1266.
 51. Saltiel, A. R., and C. R. Kahn. 2001. Insulin signalling and the regulation of glucose and lipid metabolism. *Nature* **414**:799–806.
 52. Shefi-Friedman, L., E. Wertheimer, S. Shen, A. Bak, D. Accili, and S. R. Sampson. 2001. Increased IGFR activity and glucose transport in cultured skeletal muscle from insulin receptor null mice. *Am. J. Physiol. Endocrinol. Metab.* **281**:E16–E24.
 53. Shiura, H., N. Miyoshi, A. Konishi, N. Wakisaka-Saito, R. Suzuki, K. Muguruma, T. Kohda, S. Wakana, M. Yokoyama, F. Ishino, and T. Kaneko-Ishino. 2005. *Meg1/Grb10* overexpression causes postnatal growth retardation and insulin resistance via negative modulation of the IGF1R and IR cascades. *Biochem. Biophys. Res. Commun.* **329**:909–916.
 54. Sleeman, M. W., K. E. Wortley, K. M. Lai, L. C. Gowen, J. Kintner, W. O. Kline, K. Garcia, T. N. Stitt, G. D. Yancopoulos, S. J. Wiegand, and D. J. Glass. 2005. Absence of the lipid phosphatase SHIP2 confers resistance to dietary obesity. *Nat. Med.* **11**:199–205.
 55. Smith, F. M., A. S. Garfield, and A. Ward. 2006. Regulation of growth and metabolism by imprinted genes. *Cytogenet. Genome Res.* **113**:279–291.
 56. Song, Y. H., M. Godard, Y. Li, S. R. Richmond, N. Rosenthal, and P. Delfontaine. 2005. Insulin-like growth factor I-mediated skeletal muscle hypertrophy is characterized by increased mTOR-p70S6K signaling without increased Akt phosphorylation. *J. Investig. Med.* **53**:135–142.
 57. Stein, E. G., T. A. Gustafson, and S. R. Hubbard. 2001. The BPS domain of

- Grb10 inhibits the catalytic activity of the insulin and IGF1 receptors. *FEBS Lett.* **493**:106–111.
58. **Stiles, B., Y. Wang, A. Stahl, S. Bassilian, W. P. Lee, Y. J. Kim, R. Sherwin, S. Devaskar, R. Lesche, M. A. Magnuson, and H. Wu.** 2004. Liver-specific deletion of negative regulator Pten results in fatty liver and insulin hypersensitivity. *Proc. Natl. Acad. Sci. USA* **101**:2082–2087.
59. **Vecchione, A., A. Marchese, P. Henry, D. Rotin, and A. Morrione.** 2003. The Grb10/Nedd4 complex regulates ligand-induced ubiquitination and stability of the insulin-like growth factor I receptor. *Mol. Cell. Biol.* **23**:3363–3372.
60. **Wang, J., H. Dai, N. Yousaf, M. Moussaif, Y. Deng, A. Boufelliga, O. R. Swamy, M. E. Leone, and H. Riedel.** 1999. Grb10, a positive, stimulatory signaling adapter in platelet-derived growth factor BB-, insulin-like growth factor I-, and insulin-mediated mitogenesis. *Mol. Cell. Biol.* **19**:6217–6228.
61. **Waterland, R. A., and R. L. Jirtle.** 2004. Early nutrition, epigenetic changes at transposons and imprinted genes, and enhanced susceptibility to adult chronic diseases. *Nutrition* **20**:63–68.
62. **Waterland, R. A., and R. L. Jirtle.** 2003. Transposable elements: targets for early nutritional effects on epigenetic gene regulation. *Mol. Cell. Biol.* **23**:5293–5300.
63. **Wick, K. R., E. D. Werner, P. Langlais, F. J. Ramos, L. Q. Dong, S. E. Shoelson, and F. Liu.** 2003. Grb10 inhibits insulin-stimulated insulin receptor substrate (IRS)-phosphatidylinositol 3-kinase/Akt signaling pathway by disrupting the association of IRS-1/IRS-2 with the insulin receptor. *J. Biol. Chem.* **278**:8460–8467.